nature portfolio

Peer Review File

Ultra robust negative differential resistance memristor for hardware neuron circuit implementation

REVIEWER COMMENTS

Reviewer #1 (Remarks to the Author):

This manuscript shows the NDR memristor device exhibited high reliability and temperature stability over fatigue test at high temperature. Also, this particular neural circuits generate various kinds of neural functions, which are novel. However, the author has to address following comments.

1. In the introduction section, the detailed descriptions including mechanism and advantages about NDR should be explained for clear understanding for readers.
2. In the abstract authors mentioned that the proposed NDR memristor showed high endurance exceeding 10^11 cycles. However, in the introduction section, authors mentioned 10^9 cycles for stability.
3. Please provide the fabrications details of the devices with schematics. Authors just explained the fabrications with words. It is hard to visualize how the device was made.
4. I believe the cost of this device should be more expensive than other memrister since the device fabrication requires the high vacuum equipments. I am not sure if the authors can argue that this device can reduce the hardware cost. Please explain this.
5. One of the key feature of proposed NDR memristor is high endurance (over 10^11). No data or detailed explanations can be found in the main text. Additional key results and explanations must be included in main text and main figures.
6. For the graph in Figure 1 a bottom left graph, no descriptions about 1 2 3 4 and inset figure are described.
7. The detailed explanations about hysteresis of NDR memristor should be added in the manuscript.
8. In the figure 2b which shows the air bridge structure, each component are recommended to be labeled in the SEM image. Also, the scale bar should be included.
9. In the page 7 of manuscript, the sentence “In addition, the arrangement of As atoms (yellow dots) and Ga atoms (red dots) is very regular ~”, the authors are recommended to explain how this regularly arranged atoms and lattice constants affect the property of proposed memristor.
10. In the figure 4a, authors are recommended to add and matching steps of Na K channels (1~4) the proper graph of NDR memristor output like the graph in figure 1a.
11. Please provide the specific applications of the device rather stating broad application.

Reviewer #2 (Remarks to the Author):

The paper titled “Ultra robust negative differential resistance memristor for hardware neuron circuit Implementation” would need major revision in order to be published in Nature Communications. The authors in this paper demonstrated negative differential resistance (NDR) memristor based on AlAs/In0.8Ga0.2As/AlAs quantum well with stable performance and durability. However, additional explanations regarding the performance characteristics of the proposed device in this study and their applications are required. The authors need to provide sufficient evidence to support their claims that

their study achieved remarkable results, enough to construct neuron circuits mimicking human brain functionality in a practical way or to implement novel applications in neuromorphic computing. Unfortunately, the descriptions of the figures and the connection between the device and its demonstrated applications are insufficient and lack of robustness. Therefore, the authors must provide clearer insights into how the proposed device can contribute to neuron circuit implementation.

1. In the introduction section on page 3, the authors believe that conventional memristor devices are unsatisfactory with the essential use of capacitors, limiting their practical application in neural morphological computing systems. To strengthen this paper, it would be more comprehensive if the authors detailed the specific limitations that conventional memristor devices face in these applications, particularly in relation to NDR devices. The authors need to provide more background of various devices employed in neuron circuit and why the proposed devices are more appropriated in these applications,

2. On page 3, the authors mentioned the MOVPE method has epitaxial characteristics, and that the preparation process is mature enough to have great stability. It would be great if the authors provided a more detailed explanation of the connections between the devices used in neuron circuits and the fabrication process. This would help readers better understand how these processes impact device performance and applicability in neuron circuits.

3. On page 4 and overall result-wise, the authors emphasized the durability and stability of proposed NDR devices at high temperatures. The authors might give more details on why devices in neural circuits are advantageous if they have robustness even in such harsh and high conditions.

4. The explanation of Figure 1 in the results section is insufficient, particularly regarding the detailed analysis and description of the device characteristics. Although a later section address image edge detection application, it lacks a comparison between the operation of the human brain and the neuron circuit designed to mimic it. The authors should provide a detailed analysis of how closely and accurately the neuron circuits replicate brain functionality.

5. In Figure 2, the authors employed the air bridge technology to fabricate the NDR memristor device. Does it have any advantages of air bridge in this device or any specific reason to use it? For instance, does that fabrication process contribute to the performance of devices?

6. In the introduction (pages 4) and page 7, the authors emphasize the importance of box-type hysteresis for applications in neuron circuits, noting that the demonstrated devices exhibit this hysteresis, attributed to a few vacancies in the In0.8Ga0.2As. Given that the ideal configuration of box-type hysteresis may vary depending on the application and purpose, are those amount of vacancies controllable to achieve the desired characteristic? It would help in understanding the adaptability of the device for different neuron circuit applications.

7. In Figure 3A, the authors claim that there is no obvious fluctuation with 100 cycles of scanning, however, it seems the shift towards positive way (or negative way) with those cycles. It would be great if the authors provided these shifts are acceptable or have no critical impact for further application.

8. In Figure 3f, although peak currents are unchanged as the temperature changes, it shows that the valley current increases with variable temperatures. I would appreciate it if authors provided these variations are in an acceptable range to claim they have temperature endurance.

9. Minor feedback: In line23 of page 10, “Fig. 3” needs to be Fig. 3x since it would be difficult to comprehend which figure is explained.

10. Minor feedback: In line 2 of page 11 (Apply a square wave pulse voltage at both ends of the device to generate a waveform as shown by the 4a red line…), there is no red line in Figure 4a, which might be edited in Figure or description.

11. In line 1 of page 12, it would be helpful to understand if the author provides more precise explanation of “unstable state”

12. In Figure 4, the authors demonstrated the various membrane potential process using two NDR devices. However, Figure 4 appears to present the graph of a potential process using a single NDR device. It would be more comprehensive and convincing if the authors demonstrated how two NDR devices perform together over time. Such a demonstration could show how the two devices interact to facilitate the potential process and how similarly these devices function in comparison to real neurons.

13. In Figure 5b, it would be great if the authors give more details in comparison when it comes to results since the images look comparable to each other and some of them seem to surpass those presented in this study. Clarifying these comparisons could highlight the unique contributions or potential limitations of their research.

14. In Figure 5c, the authors compared the F value from other studies with this paper. It would be more comprehensive to give more background, for example, what F-value refer to and imply. In addition, in the device level, the proposed devices show better F value than other studies did, however, when it comes to software level, F-value of software is considerably higher than the proposed device. It would make this study solid if the authors compare the software level and device level to convince the proposed devices have an advantage over software.

15. Minor feedback: In Figure 5d, it would be helpful for readers to understand if the images are labeled such as original image and image from devices.

Reviewer #3 (Remarks to the Author):

I co-reviewed this manuscript with one of the reviewers who provided the listed reports. This is part of the Nature Communications initiative to facilitate training in peer review and to provide appropriate recognition for Early Career Researchers who co-review manuscripts.

Reviewer #4 (Remarks to the Author):

The manuscript discusses the development of an ultra-robust negative differential resistance (NDR) memristor using an AlAs/In0.8Ga0.2As/AlAs quantum well structure, specifically designed for neuromorphic computing applications. This memristor is particularly noted for its high temperature resistance, high endurance, and low variation, which make it ideal for implementing hardware neuron circuits that mimic biological neuron functions. This manuscript contributes significantly to the field of neuromorphic computing, pushing the boundaries of what's possible with memristor technologies and setting a high standard for future research in this area. The integration of the NDR memristor to mimic the functionality of a neuronal membrane without the need for external capacitors is a significant advancement, potentially simplifying and reducing the cost of neuromorphic circuit design. But there are still a few issues that need to be revised and agreed to be published in Nature Communications.

1. Can the authors elaborate on the choice of the AlAs/In0.8Ga0.2As/AlAs quantum well structure over other potential materials? What specific properties of this configuration contribute to the enhanced stability and performance of the NDR memristor?
2. Given the complex fabrication process involving high-temperature epitaxial growth, how reproducible are the memristor devices across different production batches?
3. How does the device maintain its integrity and performance over prolonged exposure to harsh environmental conditions?
4. How does the simplification of the FN neuron circuit, achieved by using only two NDR memristors and an inductor, affect the circuit’s ability to replicate more complex neuron behaviors? The author can provide a more detailed description in this section.
5. There is a duplicate image between Fig S14 and Fig 5, and one of them needs to be deleted.

Dear Reviewers and Editor:

Thank you for the reviewers' comments concerning our manuscript entitled "**Ultra robust negative differential resistance memristor for hardware neuron circuit implementation**" **(NCOMMS-24-25158-A)**. Those comments are all valuable and very helpful for revising and improving our paper, as well as the important guiding significance to our research. We have studied comments carefully and have made correction which we hope meet with approval. Revised portions are marked in red in the paper. The main corrections in the manuscript and the responds to the reviewer's comments are as following:

Ⅰ. Comments from Reviewer #1

This manuscript shows the NDR memristor device exhibited high reliability and temperature stability over fatigue test at high temperature. Also, this particular neural circuits generate various kinds of neural functions, which are novel. However, the author has to address following comments.

Comment 1: In the introduction section, the detailed descriptions including mechanism and advantages about NDR should be explained for clear understanding for readers.

Response: Thank you for your suggestion. We have revised the manuscript based on your suggestions and provided a detailed description of the mechanism and advantages of negative differential resistance NDR devices.

The NDR is a characteristic of electronic devices where the current decreases as the voltage increases, which is opposite to the characteristics of conventional resistive elements. (The details of the working mechanism of NDR devices are described in Supplementary Information Section 2.) Memristors, as typical negative differential resistance (NDR) devices, commonly include conductive filament types[1], phase change types[2], and Mott types[3]. Their conduction mechanisms involve the formation and rupture of conductive filaments, transitions between crystalline and amorphous states, and Mott transitions, respectively. However, they are currently facing challenges such as the randomness of conductive filament formation and the stochastic nature of nucleation sites during phase transitions, leading to significant variability in device performance. In this work, we address these issues by constructing a resonant tunneling diode and utilizing band engineering to modulate electron/hole tunneling behavior,

thereby achieving the desired NDR characteristics in the device, which has a relatively mature preparation process and better device stability.

Manuscript revision: However, these traditional NDR memristor device are often unstable because of the randomness of conductive filament formation and phase change nucleation sites[4-6], and capacitors are usually needed to integrate neurons, which limits their practical application in large-scale neuromorphic computing systems. Therefore, it is a very necessary task to find more stable NDR devices to build neuron circuit. Fortunately, the resonant tunneling diode (RTD) is a typical NDR device that adopts band controlled tunneling mechanism and is less affected by temperature. Its preparation process is relatively mature, which makes it have better device stability[7]. Therefore, combining the NDR effect of RTD and the hysteresis characteristics of memristors is a new idea to develop suitable devices for neuron circuits.

Comment 2: In the abstract authors mentioned that the proposed NDR memristor showed high endurance exceeding 10^11 cycles. However, in the introduction section, authors mentioned 10^9 cycles for stability.

Response: We apologize for the misunderstanding caused by the expression in our manuscript. In the previous version of the manuscript, this information was presented in the supplementary information. The device has indeed demonstrated good endurance performance, reaching 10^{11} cycles at room temperature and 10^{9} cycles at 400 ℃ as shown in figure R1 in response letter. In the updated manuscript, we have adjusted this data to Figure 3. We have provided a clearer description of this performance in the manuscript and highlighted it in red.

Manuscript revision: Here, we propose an ultra-robust and efficient neuron of negative differential resistance (NDR) memristor based on AlAs/$In_{0.8}Ga_{0.2}As$/AlAs quantum well (QW) structure, which has super stable performance such as low variation (0.264%), high temperature resistance (400℃), high endurance (exceeding 10^{11} cycles at room temperature and 10^{9} cycles at 400 ℃) and neuromorphic computing.

The NDR memristor shows high reliability and temperature stability and can be cycled stably at room temperature and 10^{9} cycles at 400 ℃.

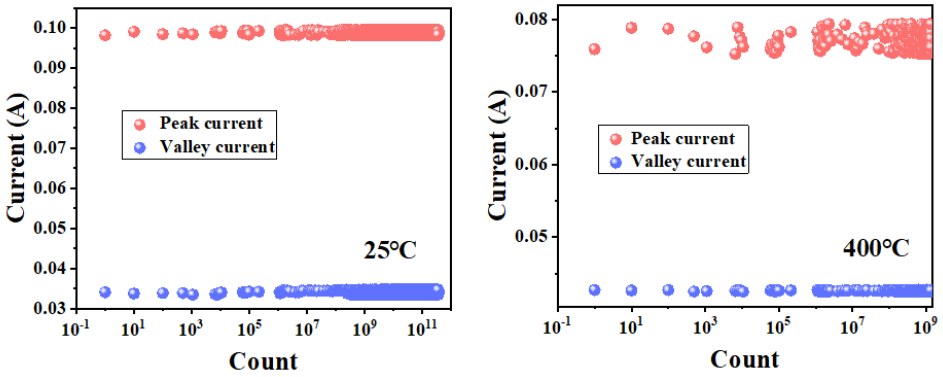

Figure R1. The NDR devices undergo more than 10^{11} switching cycles at room temperature and 10^{9} switching cycles at 400 ℃.

Comment 3: Please provide the fabrications details of the devices with schematics. Authors just explained the fabrications with words. It is hard to visualize how the device was made.

Response: Thank you for your suggestion. We have provided a detailed diagram of the device preparation process and added it to the supplementary information as shown in Figure R2.

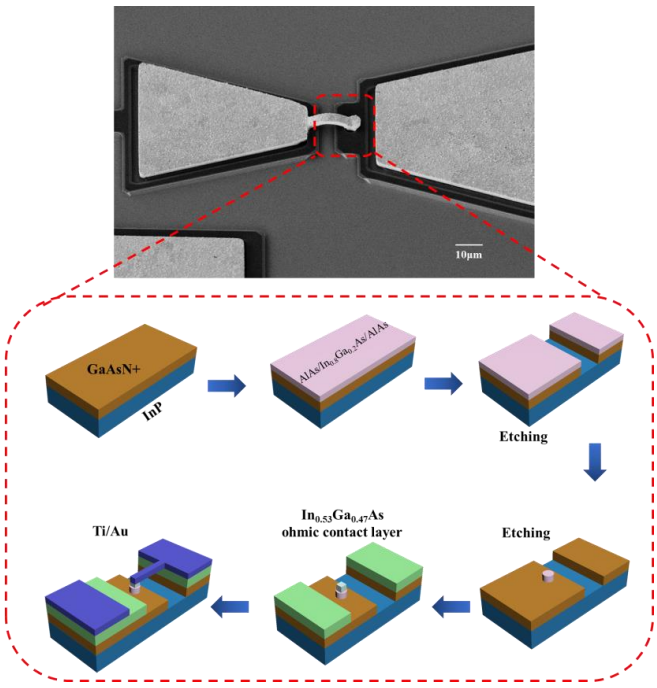

Figure R2. Process flowchart of NDR device preparation.

The epitaxy of the NDR structure consisted of a 100 nm InP buffer layer, followed by 400 nm highly n-doped GaAs (2×10^{19}cm^{-3}Si) to serve as the lower contact. Then an $In_{0.80}Ga_{0.20}As$ quantum well was formed between two AlAs barriers. The NDR structures were grown with varying QW thicknesses of 4.5 nm. The epitaxy was terminated with 15 nm n-doped

$In_{0.53}Ga_{0.47}As$ to enhance the formation of a low-resistance ohmic contact. Finally, a specific contact resistivity of 6.3 Ω/m^2 was obtained for a Ti (20 nm)/Au (200 nm) non-alloyed ohmic contact on $In_{0.53}Ga_{0.47}As$. The surface preparation procedure for the optimum contact consisted of a 10 min. O_3 treatment followed by a 15s dip in 1.25% ammonium hydroxide after which the sample was blown dry using N_2. A Ti (20 nm)/Au (200 nm) metal stack was deposited onto the samples in a metal evaporator. After the deposition, a post-metallisation anneals at 275 ˚C was carried out for the duration of 35 min. to obtain a specific contact resistivity of 6.3 Ω/m^2. These inverted air-bridge structures were fabricated on n+ InGaAs film using the photolithography mask. Metallic strips, with dimensions matching contact gaps, were created through a metal evaporation and lift-off process.

Manuscript revision (Supplementary Information Section 1): The growth was performed in a vertical Thomas Swan 6×2″ close-coupled shower head MOVPE reactor on (100) semi-insulating InP substrates with a 0.07º offcut at a pressure of 100 mTorr. A Laytec EpiTT pyrometer (calibrated using an Absolut probe) was used to control the growth temperature to 560 ˚C. The wafer was heated by three stationary resistive graphite heaters located underneath the wafer carrier which was rotated at 100 rpm in the clockwise direction. Trimethylgallium (TMG), trimethylaluminium (TMA) and trimethylindium (TMI), housed in stainless steel bubblers, were used as group-III precursors and arsine (AsH_3) and phosphine (PH_3) as the group-V source materials. Hydrogen (H_2) was used as the carrier gas and purified by a palladium cell. Epison TM gas phase analysers were used to accurately control the concentration of the gas phase. Disilane (Si_2H_6) diluted to 10 ppm in helium (He) was used as precursor to achieve n-doping concentrations. Using disilane instead of silane (SiH_4) is often preferred due to the higher silicon incorporation efficiency and lower temperature dependence. To achieve high n-doping concentrations (up to 2×10^{19} cm^{-3}), a comparatively low growth rate of 6 nm/min. was used to maximise the incorporation of the silicon dopant in the crystal. The growth rate was calibrated with the EpiTT system using optical reflectance interferometry.

The epitaxy of the NDR structure consisted of a 100 nm InP buffer layer, followed by 400 nm highly n-doped GaAs ($2\times10^{19}cm^{-3}Si$) to serve as the lower contact. An $In_{0.80}Ga_{0.20}As$ quantum well was formed between two AlAs barriers.

To minimize the parasitic capacitance of NDR devices, low resistance Ohmic contacts are

required to reduce the self-heating effect in the device, which is beneficial for optimizing device performance and reliability. The epitaxy was terminated with 15 nm n-doped $In_{0.53}Ga_{0.47}As$ to enhance the formation of a low-resistance ohmic contact. NDR structures were grown with varying QW thicknesses of 4.5 nm.

Finally, a specific contact resistivity of 6.3 Ω/m^2 was obtained for a Ti (20 nm)/Au(200 nm) non-alloyed ohmic contact on $In_{0.53}Ga_{0.47}As$. The surface preparation procedure for the optimum contact consisted of a 10 min. O_3 treatment followed by a 15s dip in 1.25% ammonium hydroxide after which the sample was blown dry using N_2. A Ti (20 nm)/Au (200 nm) metal stack was deposited onto the samples in a metal evaporator. After the deposition, a post-metallisation anneals at 275 ˚C was carried out for the duration of 35 min. to obtain a specific contact resistivity of 6.3 Ω/m^2.

These inverted air-bridge structures were fabricated on n+ InGaAs film using the photolithography mask. Metallic strips, with dimensions matching contact gaps, were created through a metal evaporation and lift-off process. Subsequently, etching of InGaAs and InP was performed using H_3PO_4:H_2O_2:H_2O (1:1:18) and HCl, respectively. This etching process formed "tunnels" beneath metallic stripes.

Comment 4: I believe the cost of this device should be more expensive than other memrister since the device fabrication requires the high vacuum equipments. I am not sure if the authors can argue that this device can reduce the hardware cost. Please explain this.

Response: Thank you for your attention to the cost issue. The simplified hardware cost here refers to the significant simplification of circuit design, which saves other hardware costs. Although it is true that using high vacuum equipment such as MOVPE for the manufacturing of NDR memristors may result in relatively high initial investment in this work, we believe that in the long run, such equipment can bring cost-effectiveness to neuromorphic computing systems.

Firstly, this circuit is only composed of two NDR memristor devices and inductance elements, which greatly reduces the complexity compared with the previous neuron circuit (Table R1). And due to the simplified design of NDR memristors, more devices can be integrated on the same chip area, which improves the utilization of silicon wafers and reduces the manufacturing cost per unit device. If more precise lithography technology at the industrial

level is adopted, the device level in the unit area will be greatly improved, which will make the single accounting cost of the device drop exponentially.[8]

Secondly, in terms of device performance, the NDR device has a switch repetition characteristic of up to 10^{11}, which makes the constructed NDR device have a longer life than other memristors, reduces the replacement cycle of the chip, and thus reduces the average annual use cost of the chip.

Thirdly, high vacuum equipment is very common in the field of integrated circuit manufacturing. For film growth equipment, most of the equipment need to carry out high vacuum extraction (including magnetron sputtering, vacuum evaporation, MOCVD, ALD, etc.) to minimize the impact of external impurities on the quality of the films. The MOVPE is a kind of equipment that uses precursors to carry organometallic compounds to the reaction chamber and then react on the surface of the substrate to form films, which makes this equipment favored for its advantages of large area growth, controllable speed, good winding, high film purity, and controllable doping concentration.[9]

Above all, although the cost of MOVPE equipment itself is high, our manufacturing process has been optimized to reduce the complexity and potential defects in the manufacturing process, thereby reducing rework and scrap rates. This NDR device can achieve more efficient computing operations, especially when dealing with large-scale datasets, which can reduce the required computing resources and energy consumption, thereby lowering overall costs.

Table R1. Compared to the complexity of neural circuits in other works.

Number of components	Neuron model	Neurons Active	Ref.
1 PCM + reset circuit	Stochastic IF	1	Nat. Nanotechnol. 2016,11, 693 (36)
14FETs + 2 capacitors	IF	4	Neural Networks. 2008, 21, 524
1MTJ+reset circuit	Stochastic IF	2	Sci. Rep. 2016, 6(1), 1-8 (35)
>100FETs+2 capacitors	FN		IEEE Trans. Neural Netw. Learn. Syst, 2019, 30(7), 2108
2 memristor+ 2 capacitors+ 2 resistor	HH	23	Nat. Commun., 2018, 9(1), 1
1 capacitors+1 resistor+1memristor	LIF	1	Nat. Commun.,2020, 11, 51
2 NDR+ 1 inductance	FN	9	This work

Comment 5: One of the key feature of proposed NDR memristor is high endurance (over 10^11). No data or detailed explanations can be found in the main text. Additional key results and explanations must be included in main text and main figures.

Response: Thank you for your professional suggestion. Originally, we presented the data on device high endurance (over 10^{11}) in the supplementary information. Based on your suggestion, we presented the key data in the main text and provided relevant descriptions in the manuscript as shown in Figure R1.

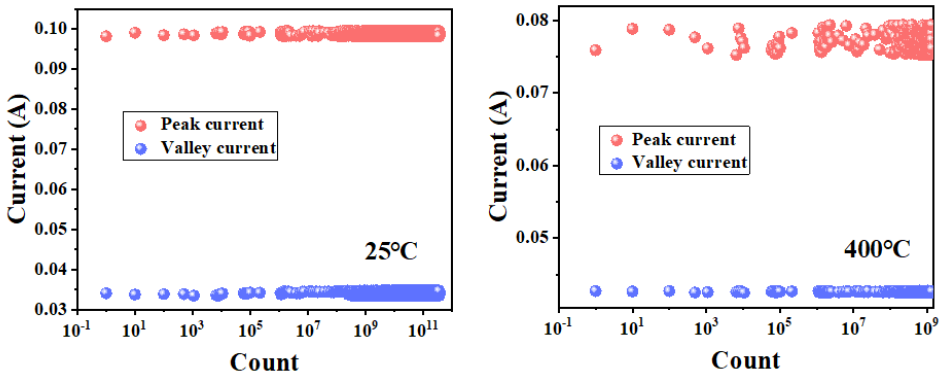

Figure R1. The NDR devices undergo more than 10^{11} switching cycles at room temperature and 10^9 switching cycles at 400 °C.

Manuscript revision: Fig. 3e shows that NDR devices can cycle more than 10^{11} switching cycles at room temperature and Fig. 3f shows that NDR devices can cycle more than 10^9 switching cycles even at a high temperature of 400 °C, which means that the device can operate for more than 310 years at 10 Hz update frequency.

Comment 6: For the graph in Figure 1 a bottom left graph, no descriptions about 1 2 3 4 and inset figure are described.

Response: Thank you for your professional advice. For better understanding by readers, we have adjusted the action potential schematic diagram to Figure 4a (Figure R3), which corresponds more clearly with the ion channel working schematic diagram of the four stages.

In Figure 4a, 1, 2, 3, and 4 express four stages of action potential, namely 1, Resting state, both Na^+ and K^+ channels are closed. 2, Depolarization, the depolarization caused by the activation of Na^+ channels make the membrane potential move in the positive direction. 3, Re- and hyper-polarization, the Re- and hyper-polarization caused by the activation of K^+ channel drives the membrane potential to the negative direction. 4, Refractory period, neurons are recovering and have no response to another stimulus.[10]

Figure R3. a, Four dynamical events during the electrical impulse (1–4) are marked. 1, Resting state. 2, Depolarization. 3, Re- and hyper-polarization. 4, Refractory period.

Manuscript revision: An action potential in a biological neuron consists of three events, corresponding to four states as shown in Fig.4a. Among them, 1, 2, 3, and 4 express four stages of action potential, namely 1, Resting state, both Na^+ and K^+ channels are closed. 2, Depolarization, the depolarization caused by the activation of Na^+ channels make the membrane potential move in the positive direction. 3, Re- and hyper-polarization, the Re- and hyper-polarization caused by the activation of K^+ channel drives the membrane potential to the negative direction. 4, Refractory period, neurons are recovering and have no response to another stimulus.[10]

Comment 7: The detailed explanations about hysteresis of NDR memristor should be added in the manuscript.

Response: Thank you for your suggestion. We have added the detailed explanations about hysteresis of NDR memristors to the manuscript. In the negative differential resistance (NDR) devices, the application of an external voltage facilitates electron tunneling within the device's structure, leading to the generation of a tunneling current.[11] Due to the control of the number of vacancies during material growth, which become electron capture centers during the conductive process. This capture center can capture electrons, and when the current decreases, the captured electrons are released, resulting in a hysteresis phenomenon.[12](Figure R4)

Manuscript revision: In the negative differential resistance (NDR) devices, the application of an external voltage facilitates electron tunneling within the device's structure, leading to the generation of a tunneling current.[11] Due to internal defects in semiconductor materials, electrons are captured, resulting in a certain accumulation of electrons at the interface. This accumulation of electrons will reduce the energy band at the interface. When the current decreases, the captured electrons are released, resulting in a hysteresis phenomenon.[12] Therefore, as the voltage decreases, the switching voltage will decrease to a certain extent and a certain window will appear (Fig. 3b).

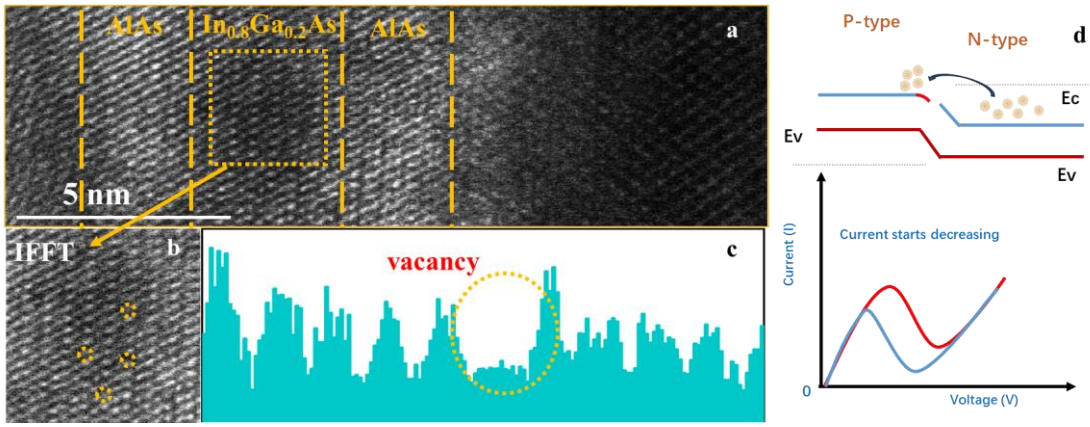

Figure R4. a, High resolution TEM image of QW structure in (a). **b**, In the inverse FFT image of $In_{0.8}Ga_{0.2}As$, it can clearly see the defects marked in the yellow circle. **c**, Line profiles of the areas with and without atomic vacancies in $In_{0.8}Ga_{0.2}As$. **d**, The working mechanism of NDR memristor devices.

Comment 8: In the figure 2b which shows the air bridge structure, each component are recommended to be labeled in the SEM image. Also, the scale bar should be included.

Response: Thank you for reminding me. We added a scale bar to the original image. Due to the thin thickness of AlAs/$In_{0.8}Ga_{0.2}As$/AlAs, it is not easy to label. Therefore, we have drawn a schematic cross-sectional diagram of the device in Fig. R5a, and the SEM image in Fig. R5b shows the structure of the yellow circle in a.

Manuscript revision: Fig. 2b is the SEM image of the yellow circle in Fig. 2a. The process details are described in detail in the Supplementary Information (Section 1) as shown in Fig. S2.

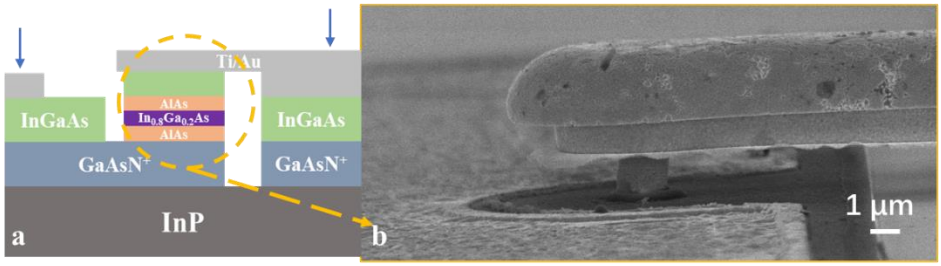

Figure R5. The SEM image of air bridge structure.

Comment 9: In the page 7 of manuscript, the sentence "In addition, the arrangement of As atoms (yellow dots) and Ga atoms (red dots) is very regular ~", the authors are recommended to explain how this regularly arranged atoms and lattice constants affect the property of proposed memristor.

Response: The neat arrangement of As and Ga atoms in TEM images proves that GaAs thin films have good film quality and epitaxial structure, which can reduce the formation of

interface states between GaAs layers and AlAs layers, as well as between GaAs layers and InP substrates.[13] High quality interfaces can reduce carrier scattering and capture, thereby reducing the contact resistance of the device and improving carrier injection efficiency.[14] In addition, high-quality GaAs layers typically have better thermal conductivity and thermal expansion matching, which helps reduce thermal stress and thermal gradient, and can also improve the overall thermal stability of the device.[15] Therefore, good film quality is beneficial for manufacturing more efficient, stable, and reliable memristors.

Manuscript revision: The Fig. S3 in Supplementary Information shows that the arrangement of As atoms (yellow dots) and Ga atoms (red dots) is very regular, and the lattice constants are 3.76Å and 3.48Å, which can reduce the formation of interface states between GaAs layers and AlAs layers, as well as between GaAs layers and InP substrates. As shown in Fig. 2f, the TEM image of the enlarged cross section of AlAs/$In_{0.8}Ga_{0.2}As$/AlAs QW shows the layer-by-layer growth of the film with good interfaces between AlAs and $In_{0.8}Ga_{0.2}As$. Excellent film quality not only reduces the formation of interfacial states between layers, but also has better thermal conductivity and thermal expansion matching, which helps to reduce thermal stress and thermal gradient, and improve the overall thermal stability of the device. [14,15]

Comment 10: In the figure 4a, authors are recommended to add and matching steps of Na K channels (1~4) the proper graph of NDR memristor output like the graph in figure 1a.

Figure R3. a, Four dynamical events during the electrical impulse (1–4) are marked. 1, Resting state. 2, Depolarization. 3, Re- and hyper-polarization. 4, Refractory period.

Response: Thank you for your suggestion. For readers to better understand, we have moved the graph of action potential changes in Fig1 a to Fig4 a. The four processes correspond to, 1, Resting state. 2, Depolarization. 3, Re- and hyper-polarization. 4, Refractory period.[10]

Here we will provide a detailed description of the working process of the circuit and its association with neurons. In the resting state, both Device 1 (D1) and Device 2 (D2) are in the low resistance state. When subjected to an input voltage stimulation exceeding the threshold, D1 enters the high resistance state, causing the membrane potential to rise and exhibit

depolarization behavior. Subsequently, the increase in membrane potential triggers D2 to enter the high resistance state, causing the membrane potential to further increase (further depolarization). Then the current flowing through the inductor decreases, the voltage (membrane potential) on both D1 and D2 decreases. Once the voltage drops below the hold value of D2, the D2 goes back to a low resistance state and speeds up the decrease of membrane potential. Once the voltage drops below the hold voltage of D1, the D1 goes back to the low resistance state, the membrane potential further decreases and drops to a negative value, corresponding to re-polarization and hyperpolarization. It should be noted that, the hold voltage of D2 is higher than the threshold voltage of D1, just as the stages shown in Fig. R3a. At this point, both D1 and D2 return to the initial. Due to the presence of inductance, the membrane potential slowly returns to the resting potential, corresponding to the refractory period in an action potential.

Manuscript revision: An action potential in a biological neuron consists of three events, corresponding to four states as shown in Fig.4a. The four processes correspond to, 1, Resting state. 2, Depolarization. 3, Re- and hyper-polarization. 4, Refractory period.

Comment 11: Please provide the specific applications of the device rather stating broad application.

Response: Thank you for your professional suggestion. Based on the high temperature stability characteristics of the device, we designed a voltage-temperature multi-modal spiking neural network, because of the differences in the response curves of the neuron circuit at different temperatures in terms of input voltage and output frequency, we processed the dataset to introduce information about the temperature dimension to the images, and processed the MNIST dataset into 20 classes (ten different numbers, two different temperatures), and used the voltage-temperature multi Modal Impulse Neural Network to go through the training and ended up with an accuracy of 91.74%, which is much higher than the training accuracy when training the network with only voltage signals.

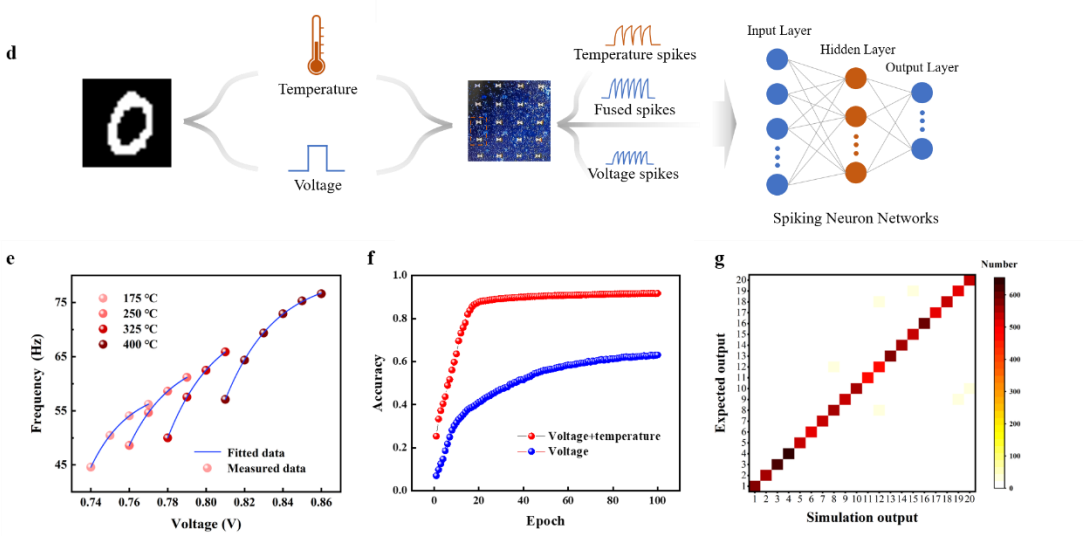

Figure R6 d, Schematic diagram of voltage-temperature multimodal image recognition system. **e**, Input voltage versus output frequency curves at four different temperatures. **f**, Accuracy of the network after 100 epochs using only voltage mode and voltage-temperature fusion mode. **g**, Confusion matrix of real and desired outputs in voltage-temperature fusion mode.

Manuscript revision: Meanwhile, a voltage-temperature fused multimodal spiking neural network system was constructed using FN neurons based on the high-temperature stability characteristics of the device, as shown in Fig. 5d. The MNIST dataset was processed and temperature information was introduced, the specific processing is shown in Supplementary Information (Section 2.4). Then the image pixel information was mapped as the input voltage to the FN neurons, and the spiking signals fusing the voltage and the temperature were obtained after neuron processing, and then entered a spiking neural network for classification, with a network structure of 28*28 neurons in the input layer, 128 neurons in the hidden layer, and the output layer of 20 neurons. Fig. 5e displays the curves of the relationship between the input voltage and the output frequency for four temperatures, where the output frequency gradually increases as the temperature increases, thus allowing easy decoupling of the temperature and pressure information in the fusion spikes. Under the same network structure, the results of training with voltage spikes signals alone and voltage-temperature fused spikes signals respectively are shown in Fig. 5f. After 100 epochs of training, the accuracy of the network trained with voltage-temperature fused spikes signals reaches 91.74%, while the accuracy of the network trained with voltage spikes signals alone is only 63.1%. Fig. 5g shows the confusion matrix heat map of the network trained by voltage-temperature fusion spikes, which shows that the network achieves excellent classification results and only few samples are

misclassified. In summary, it is proved by simulation that our system can complete the classification of images at high temperatures, and at the same time, it can distinguish between different temperatures.

Ⅱ. Comments from Reviewer #2

The paper titled “Ultra robust negative differential resistance memristor for hardware neuron circuit Implementation” would need major revision in order to be published in Nature Communications. The authors in this paper demonstrated negative differential resistance (NDR) memristor based on AlAs/In0.8Ga0.2As/AlAs quantum well with stable performance and durability. However, additional explanations regarding the performance characteristics of the proposed device in this study and their applications are required. The authors need to provide sufficient evidence to support their claims that their study achieved remarkable results, enough to construct neuron circuits mimicking human brain functionality in a practical way or to implement novel applications in neuromorphic computing. Unfortunately, the descriptions of the figures and the connection between the device and its demonstrated applications are insufficient and lack of robustness. Therefore, the authors must provide clearer insights into how the proposed device can contribute to neuron circuit implementation.

Comment 1: In the introduction section on page 3, the authors believe that conventional memristor devices are unsatisfactory with the essential use of capacitors, limiting their practical application in neural morphological computing systems. To strengthen this paper, it would be more comprehensive if the authors detailed the specific limitations that conventional memristor devices face in these applications, particularly in relation to NDR devices. The authors need to provide more background of various devices employed in neuron circuit and why the proposed devices are more appropriated in these applications

Response: Thank you for your professional suggestions. Based on your suggestions, we have improved and revised the introduction section of the manuscript, explaining the limitations faced by traditional memristor devices and NDR devices in neural circuit applications, and providing more background on the various devices used in neural circuits. The revised section is marked in red in the manuscript.

On the one hand, from the perspective of devices, the conductive filament type NDR memristors rely on the non-uniformity of internal ion distribution, and the phase change materials rely on the in crystal structure, which makes the devices difficult to achieve high stability and uniformity[16-18]. This NDR memristor device is an electronic behavior controlled

by energy band. The electronic resonance tunneling behavior used in the switching process of the device does not change the distribution of internal ions and crystal structure, so it can improve the stability of the device and make the device more uniform.[19,20]

On the other hand, the Fitz Hugh Nagumo (FN) neuron circuit constructed by NDR memristor effectively demonstrates the feasibility and advantages of designing neuron circuits without using capacitors. This design not only reduces hardware costs, but also enables diverse neuronal dynamics and functions, providing a new approach for developing high-performance neuromorphic hardware systems. Firstly, omitting capacitors can make circuit design more concise, reduce the number of components, and thus reduce the overall complexity of the design. More neural circuits can be integrated in the same space, which is very beneficial for the development of high-density neuromorphic computing systems. And the simplified circuit design is easier to expand to larger scale neural networks, which helps to achieve more complex neuromorphic computing tasks. Secondly, the NDR memristor itself has bistable characteristics, which can quickly switch between two states without the need for capacitors for charging and discharging, thereby potentially improving the response speed of the circuit. The negative differential resistance characteristic of NDR memristor allows it to naturally replicate the oscillatory behavior of neurons, which is crucial for processing time-varying signals.

Manuscript revision: Among them, negative differential resistance (NDR) memristor neurons have aroused the greatest interest, including threshold switch memristors[1], phase change memristors (PCM)[2], Mott memristors[3], etc. However, these traditional NDR memristor device are often unstable because of the randomness of conductive filament formation and phase change nucleation sites[4-6], and capacitors are usually needed to integrate neurons, which limits their practical application in large-scale neuromorphic computing systems. Therefore, it is a very necessary task to find more stable NDR devices to build neuron circuit. Fortunately, the resonant tunneling diode (RTD) is a typical NDR device with band controlled tunneling, and its preparation process is relatively mature, which makes it have better device stability[7]. Therefore, combining the NDR effect of RTD and the hysteresis characteristics of memristors is a new idea to develop suitable devices for neuron circuits.

The NDR memristor is used to construct a simple Fitz Hugh Nagumo (FN) neuron circuit, which effectively proves the feasibility and advantages of designing neuron circuit without

capacitor. This design not only reduces hardware costs but also enables diverse neuron dynamics and functionality.

Comment 2: On page 3, the authors mentioned the MOVPE method has epitaxial characteristics, and that the preparation process is mature enough to have great stability. It would be great if the authors provided a more detailed explanation of the connections between the devices used in neuron circuits and the fabrication process. This would help readers better understand how these processes impact device performance and applicability in neuron circuits.

Response: Thank you for your suggestions. The Metal Organic Vapor Epitaxy (MOVPE) method is used to grow high-quality InP and GaAsN+ based epitaxial layers, which has a mature preparation process and good equipment stability. MOVPE technology allows for precise control of material growth at the atomic level, which is crucial for achieving high-uniformity electronic devices. In neural morphological computing systems, the performance and applicability of devices are directly affected by their preparation process. The above preparation process enables us to achieve very good device performance, such as high-quality epitaxial layers that reduce lattice mismatch and defects, thereby improving the uniformity and reliability of the device. The device shows only a 0.29 % temporal variation (σ/μ) during 100 consecutive DC cycles, which is nearly 5 times higher than the currently reported high reliability devices[21]. We have described the device preparation process in more detail in the supplementary information of the new manuscript, as shown in Figure R2.

The growth was performed in a vertical Thomas Swan 6×2″ close-coupled shower head MOVPE reactor on (100) semi-insulating InP substrates with a 0.07° offcut at a pressure of 100 mTorr. A Laytec EpiTT pyrometer (calibrated using an Absolut probe) was used to control the growth temperature to 560 ˚C. The wafer was heated by three stationary resistive graphite heaters located underneath the wafer carrier which was rotated at 100 rpm in the clockwise direction. Trimethylgallium (TMG), trimethylaluminium (TMA) and trimethylindium (TMI), housed in stainless steel bubblers, were used as group-III precursors and arsine (AsH_3) and phosphine (PH_3) as the group-V source materials. Hydrogen (H_2) was used as the carrier gas and purified by a palladium cell. Epison TM gas phase analysers were used to accurately control the concentration of the gas phase. Disilane (Si_2H_6) diluted to 10 ppm in helium (He) was used as precursor to achieve n-doping concentrations. Using disilane instead of silane (SiH_4) is often

preferred due to the higher silicon incorporation efficiency and lower temperature dependence. To achieve high n-doping concentrations (up to 2×10^{19} cm^{-3}), a comparatively low growth rate of 6 nm/min. was used to maximise the incorporation of the silicon dopant in the crystal. The growth rate was calibrated with the EpiTT system using optical reflectance interferometry.

The epitaxy of the NDR structure consisted of a 100 nm InP buffer layer, followed by 400 nm highly n-doped GaAs ($2\times10^{19}cm^{-3}Si$) to serve as the lower contact. An $In_{0.80}Ga_{0.20}As$ quantum well was formed between two AlAs barriers.

To minimize the parasitic capacitance of NDR devices, low resistance Ohmic contacts are required to reduce the self-heating effect in the device, which is beneficial for optimizing device performance and reliability. The epitaxy was terminated with 15 nm n-doped $In_{0.53}Ga_{0.47}As$ to enhance the formation of a low-resistance ohmic contact. NDR structures were grown with varying QW thicknesses of 4.5 nm.

Finally, a specific contact resistivity of 6.3 Ω/m^2 was obtained for a Ti (20 nm)/Au(200 nm) non-alloyed ohmic contact on $In_{0.53}Ga_{0.47}As$. The surface preparation procedure for the optimum contact consisted of a 10 min. O_3 treatment followed by a 15s dip in 1.25% ammonium hydroxide after which the sample was blown dry using N_2. A Ti (20 nm)/Au (200 nm) metal stack was deposited onto the samples in a metal evaporator. After the deposition, a post-metallisation anneal at 275 ˚C was carried out for the duration of 35 min. to obtain a specific contact resistivity of 6.3 Ω/m^2.

These inverted air-bridge structures were fabricated on n+ InGaAs film using the photolithography mask. Metallic strips, with dimensions matching contact gaps, were created through a metal evaporation and lift-off process. Subsequently, etching of InGaAs and InP was performed using H_3PO_4:H_2O_2:H_2O (1:1:18) and HCl, respectively. This etching process formed "tunnels" beneath metallic stripes.

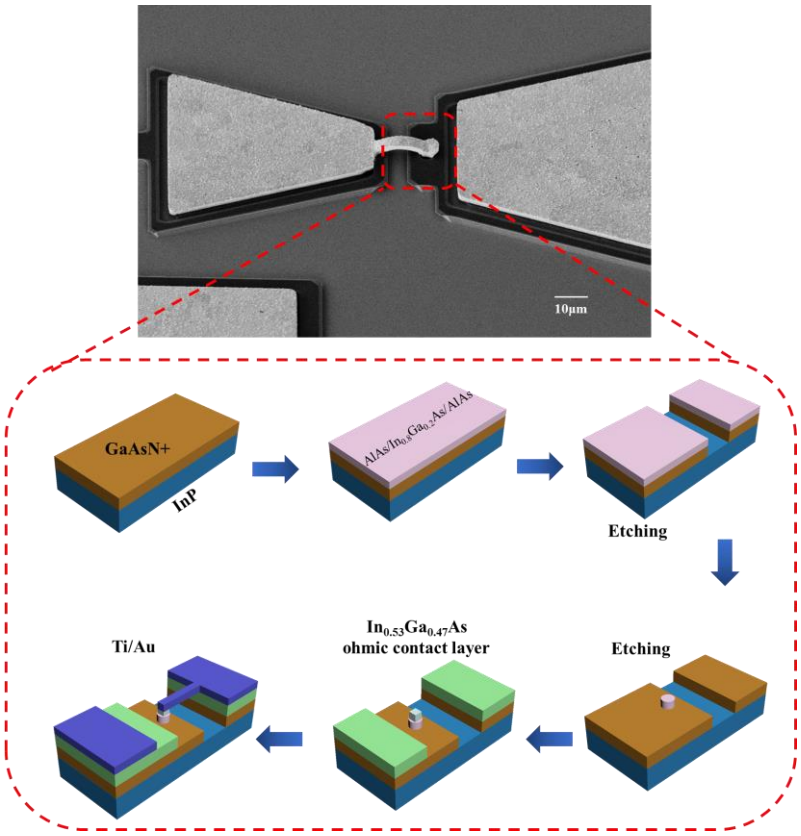

Figure R2. Process flowchart of NDR device preparation.

Comment 3: On page 4 and overall result-wise, the authors emphasized the durability and stability of proposed NDR devices at high temperatures. The authors might give more details on why devices in neural circuits are advantageous if they have robustness even in such harsh and high conditions.

Response: The good robustness of the NDR memristor device under high temperature conditions is due to the careful control of the process conditions by the AlAs/$In_{0.8}Ga_{0.2}$As/AlAs quantum well structure design and growth process. Firstly, the AlAs/$In_{0.8}Ga_{0.2}$As/AlAs quantum well structure of NDR devices has been carefully selected to have high thermal stability. The bandgap and lattice constants of these materials are designed to maintain their electronic structure and properties unchanged at high temperatures.[22,23] Moreover, the quantum tunneling process is relatively unaffected by temperature induced lattice vibrations, thus maintaining stable current voltage (I-V) characteristics even at high temperatures.[24] In the AlAs/$In_{0.8}Ga_{0.2}$As/AlAs quantum well structure, electrons undergo resonant tunneling through a double barrier structure. Resonant tunneling can achieve efficient electron transfer at specific energy levels, which is insensitive to temperature changes and helps maintain stability at high temperatures.[25] Although high temperatures may increase lattice vibrations and lead to

increased scattering, temperature assisted tunneling in quantum wells can overcome this problem, as the increased temperature helps electrons tunnel through higher resonance levels, thereby maintaining NDR characteristics.

Finally, we designed a voltage-temperature multimodal image recognition system, which fuses the spike signals of image pixel values and temperatures to classify them through a spike neural network, and the results show that the system produces good classification results for different numbers with different temperature labels at high temperatures.

Manuscript revision: The excellent robustness of NDR memristor devices under high temperature conditions can be attributed to the high thermal stability of the AlAs/$In_{0.8}Ga_{0.2}As$/AlAs quantum well structure. By using a double barrier structure for resonant tunneling, efficient electron transfer can be achieved at specific energy levels, which is insensitive to temperature changes and helps maintain stability at high temperatures.

Comment 4: The explanation of Figure 1 in the results section is insufficient, particularly regarding the detailed analysis and description of the device characteristics. Although a later section address image edge detection application, it lacks a comparison between the operation of the human brain and the neuron circuit designed to mimic it. The authors should provide a detailed analysis of how closely and accurately the neuron circuits replicate brain functionality.

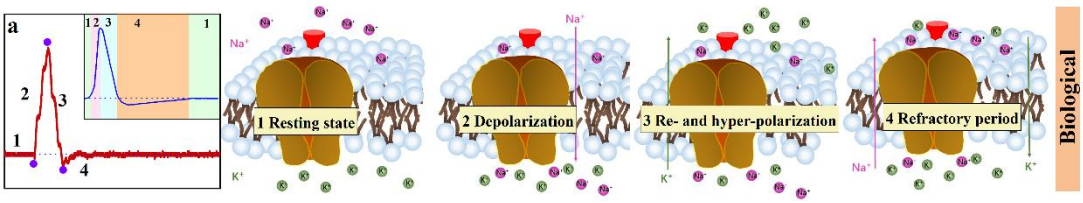

Figure R3.a, Four dynamical events during the electrical impulse (1–4) are marked. 1, Resting state. 2, Depolarization. 3, Re- and hyper-polarization. 4, Refractory period.

Response: Thank you for your question. The human brain has 10^{11} neurons and 10^{15} synapses, which can integrate complex brain functions such as perception, computation, logic, language, vision, and memory[26]. Neurons are the basic working units of the nervous system, capable of receiving signals from other neurons and processing them. In this work, the FN neuron circuit constructed based on NDR has close similarities with biological neurons in the working process.

Here we will provide a detailed description of the working process of the circuit and its association with neurons. In the resting state, both Device 1 (D1) and Device 2 (D2) are in the

low resistance state. When subjected to an input voltage stimulation exceeding the threshold, D1 enters the high resistance state, causing the membrane potential to rise and exhibit depolarization behavior. Subsequently, the increase in membrane potential triggers Device 2 to enter the high resistance state, causing the membrane potential to further increase (further depolarization). Then the current flowing through the inductor decreases, the voltage (membrane potential) on both D1 and D2 decreases. Once the voltage drops below the hold value of D2, the D2 goes back to a low resistance state and speeds up the decrease of membrane potential. Once the voltage drops below the hold voltage of D1, the D1 goes back to the low resistance state, the membrane potential further decreases and drops to a negative value, corresponding to re-polarization and hyperpolarization. It should be noted that, the hold voltage of D2 is higher than the threshold voltage of device 1, just as the stages shown in Fig. R3a. At this point, both D1 and D2 return to the initial. Due to the presence of inductance, the membrane potential slowly returns to the resting potential, corresponding to the refractory period in an action potential.

Manuscript revision: An action potential in a biological neuron consists of three events, corresponding to four states as shown in Fig.4a. The four processes correspond to, 1, Resting state. 2, Depolarization. 3, Re- and hyper-polarization. 4, Refractory period.

Comment 5: In Figure 2, the authors employed the air bridge technology to fabricate the NDR memristor device. Does it have any advantages of air bridge in this device or any specific reason to use it? For instance, does that fabrication process contribute to the performance of devices?

Response: Since the FN neuron circuit designed in this work is a high-frequency oscillation circuit, it is necessary to minimize the device capacitance. This design not only reduces parasitic capacitance but also reduces interconnect resistance. The air bridge provides a low capacitance connection method because it avoids direct contact between metal layers, thereby reducing the impact of parasitic capacitance.[27,28] This is crucial for high-speed neuromorphic computing systems, as parasitic capacitance limits the frequency response of the signal.[29] In addition, as the air bridge reduces the bending and length of metal wires, it can lower the interconnect resistance, which is crucial for improving signal transmission efficiency and reducing power consumption.[30]This design can also improve the thermal stability and

performance of the device. The air bridge structure, due to its low thermal conductivity, helps to isolate heat sources and reduce the impact of heat on device performance.[27] This is particularly important under high-temperature operating conditions as it helps maintain the stability of the device.

Comment 6: In the introduction (pages 4) and page 7, the authors emphasize the importance of box-type hysteresis for applications in neuron circuits, noting that the demonstrated devices exhibit this hysteresis, attributed to a few vacancies in the In0.8Ga0.2As. Given that the ideal configuration of box-type hysteresis may vary depending on the application and purpose, are those amount of vacancies controllable to achieve the desired characteristic? It would help in understanding the adaptability of the device for different neuron circuit applications.

Response: Your consideration is completely correct. The vacancies in In0.8Ga0.2As are controllable, and their quantity and distribution can be controlled by adjusting growth conditions or subsequent process steps. Furthermore, the box-type hysteresis characteristics can be adjusted to meet the needs of different neural circuits. This is mainly due to the use of in-situ monitoring technology during the growth process. By using in-situ monitoring technology during the growth process, the growth of the thin film can be observed in real time, and the growth conditions can be adjusted based on feedback to achieve control of the number of vacancies. In terms of specific experimental operations, it is first necessary to precisely control the growth temperature. Growth is carried out at 560° C, which is conducive to the formation of a flat and uniform epitaxial layer of In and Ga atoms on an InP substrate, while reducing potential thermal defects caused by high temperatures. By introducing disilane (Si_2H_6) diluted in helium (He) as a doping source during the growth process, high n-type doping concentration can be achieved. The growth rate is set at 6 nanometers per minute, which is relatively low and helps to improve the solubility of silicon dopants in the crystal, while allowing more time for ordered atomic arrangement. Real time monitoring and calibration of growth rate are achieved through optical reflection interferometry measurement technology, ensuring the accuracy and repeatability of the growth process.

Comment 7: In Figure 3A, the authors claim that there is no obvious fluctuation with 100 cycles of scanning, however, it seems the shift towards positive way (or negative way) with

those cycles. It would be great if the authors provided these shifts are acceptable or have no critical impact for further application.

Response: NDR memristor shows extremely high stability, and 0.29 % temporal variation (σ/μ) shows its excellent consistency and reliability during 100 consecutive DC cycles, which is nearly 5 times higher than the currently reported high reliability devices[21]. In the 100 cycles of scanning, the range of switch voltage fluctuations is also very small and follows a Gaussian distribution of random fluctuations, and will not have a significant impact on the overall performance of the device as shown in Fig. R7. In many cases, small fluctuations may be due to natural phenomena in the process of electron transmission, such as electron scattering, which have limited impact on circuit performance without significantly changing I-V characteristics.[31] As long as the threshold voltage of D2 is bigger than the threshold voltage of D1, the circuit can operate normally. This fluctuation can serve as an intrinsic source of randomness for neural circuits, and instead contribute to enhancing the robustness of the system.[32]

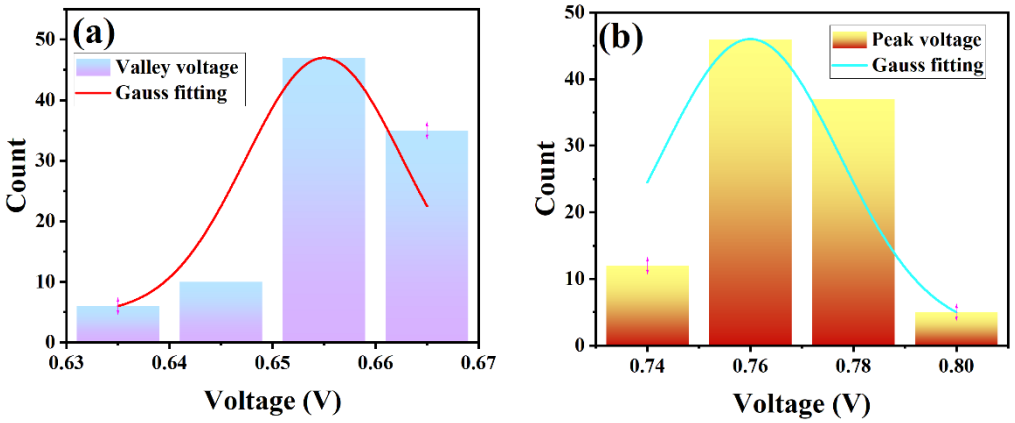

Figure R7. Statistical data of Gaussian fitted histograms of peak voltage and valley voltage of devices.

Comment 8: In Figure 3f, although peak currents are unchanged as the temperature changes, it shows that the valley current increases with variable temperatures. I would appreciate it if authors provided these variations are in an acceptable range to claim they have temperature endurance.

Response: The range of current variation in this work is acceptable and still meets the requirements of circuit design. At 400 °C, the NDR memristor shows 0.12% temporal variation (σ/μ) shows its excellent consistency and reliability during 100 consecutive DC cycles. In addition, neuromorphic circuit design usually has a certain tolerance and can adapt to certain changes in device parameters without significantly affecting circuit performance. And all

devices exhibit consistent behavior under temperature changes, even if there are changes, the overall performance of the circuit can be optimized through design.

Comment 9: Minor feedback: In line23 of page 10, “Fig. 3” needs to be Fig. 3x since it would be difficult to comprehend which figure is explained.

Response: Thanks for your reminding, we modified the manuscript and marked it as fig.3j.

Manuscript revision: Fig. 3j shows the peak to valley current and peak to valley voltage variation of NDR devices at 25 ℃ - 400 ℃.

Comment 10: Minor feedback: In line 2 of page 11 (Apply a square wave pulse voltage at both ends of the device to generate a waveform as shown by the 4a red line…), there is no red line in Figure 4a, which might be edited in Figure or description.

Response: For better understanding, we moved the image to Fig 4a, deleted this sentence in its original position, and described it in Fig 4a. The red line in the figure represents the output waveform of the FN neuron circuit, while the blue line represents the waveform of the biological action potential. The circuit output can simulate the biological action potential very well.

Comment 11: In line 1 of page 12, it would be helpful to understand if the author provides more precise explanation of “unstable state”

Response: We apologize that our expression did not allow readers to understand clearly. Here, "unstable state" means the NDR device working state is in the hysteresis range (Figure R5). To provide readers with a clearer understanding, we have revised the manuscript to " In the resting state, both the Na^+ and K^+ channels are closed, both Device 1 and Device 2 are in the low resistance state."

Comment 12: In Figure 4, the authors demonstrated the various membrane potential process using two NDR devices. However, Figure 4 appears to present the graph of a potential process using a single NDR device. It would be more comprehensive and convincing if the authors demonstrated how two NDR devices perform together over time. Such a demonstration could show how the two devices interact to facilitate the potential process and how similarly these devices function in comparison to real neurons.

Response: Thank you for your professional suggestions. We added a neural circuit to generate a spike image of action potential as shown in Fig4a. And demonstrated the working

process of two devices to correspond to the neuronal Na^+ and K^+ channels. The collaborative process of two NDR devices in neural morphological circuits is significantly like the generation and propagation of action potentials in real neurons. In real neurons, the generation of action potentials is caused by the dynamic opening and closing of voltage-gated sodium and potassium ion channels, while the depolarization and hyperpolarization stages are controlled by the flow of sodium and potassium ions, respectively. Similarly, in our circuit, two NDR devices simulate the behavior of these ion channels: 1. In the resting state, both devices are in a LRS state, which corresponds to the resting state of neuronal membrane potential. 2. The depolarization, when the input voltage exceeds the oscillation voltage of D1, which will be triggered to the oscillation state. Due to the voltage division principle between the device and the inductor, the node voltage will increase, and D2 will be triggered to the oscillation state, causing the node voltage to rise again. 3. Afterwards, due to the presence of inductance, the node voltage will gradually decrease until D2 can be converted back to LRS. This will lead to a decrease in the partial voltage of the device, and the node voltage will also decrease, causing the state of D1 to return to LRS. At this point, the node voltage will become negative, corresponding to the processes of repolarization and hyperpolarization. 4. Because of inductance, the node voltage will slowly return to the resting potential. This corresponds to the refractory period. By precisely adjusting the characteristics of NDR devices, multiple discharge behaviors and the integration and synchronous oscillation behavior of complex neural networks can be achieved.

Comment 13: In Figure 5b, it would be great if the authors give more details in comparison when it comes to results since the images look comparable to each other and some of them seem to surpass those presented in this study. Clarifying these comparisons could highlight the unique contributions or potential limitations of their research.

Response: Sorry, our expression is difficult for readers to understand. Based on the suggestions of Reviewer 1, we have highlighted the unique advantages of the device and rephrased this section to help readers better understand. Firstly, when comparing with other neurons, the comparison is made using the same way as other neurons edge detection shape, i.e. the way shown in Fig. 5a, and finally the F-Measure obtained by our device is higher than that of the other neuron circuits, whereas, when comparing with the software operators, we have obtained edge detection results with different operators under different operators. The

edge detection results were obtained with our FN neuron circuit and software respectively, and the details of the comparison are given in Figure 5c, the results obtained were compared using SSIM and PSNR and the results showed that the FN neuron based edge detection results under multiple operators produced only a small amount of error compared to the software, which is acceptable.

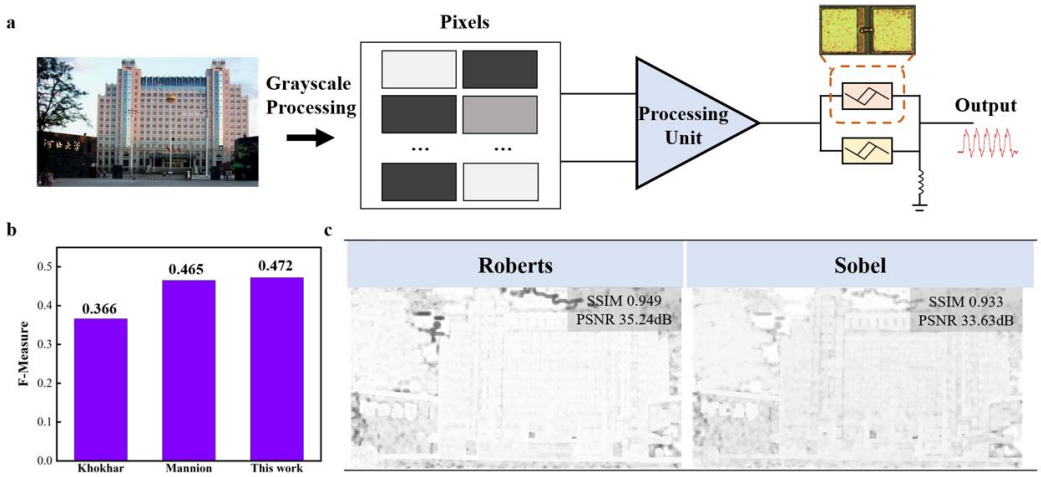

Figure R8. **a**, Schematic representation of the principle of edge detection by FN neurons. **b**, Comparative analysis of edge detection performance based on the BSDS500 dataset. **c**, Metrics evaluation of edge detection images using SSIM and PSNR.

Manuscript revision:

Meanwhile, the FN neuron circuit performed the edge detection work using the same way as the software operator, which is the convolutional edge detection method. The edge detection was compared using two evaluation metrics, SSIM and PSNR, and the principle is demonstrated in Supplementary Information (Section 2.3). The results show that the neuron-based edge detection compared to the software operator results in SSIM of 0.949 (Roberts) and 0.933 (Sobel), shown in Fig. 5c respectively, which produces a small amount of error, but this result is acceptable. On the one hand, the software simulation is performed using a CPU for the convolution operation, which consumes about 0.0638J of energy per convolutional computation, whereas the neuronal circuits consume 4-5 orders of magnitude less energy than the CPU for the same criteria. On the other hand, this FN neuron circuit is a basic unit circuit that can be easily embedded into other circuits to form more complex neuromorphic computing circuits to perform various real-time computational tasks, which cannot be accomplished by traditional computing chips such as CPUs.

Comment 14: In Figure 5c, the authors compared the F value from other studies with this paper. It would be more comprehensive to give more background, for example, what F-value refer to and imply. In addition, in the device level, the proposed devices show better F value than other studies did, however, when it comes to software level, F-value of software is considerably higher than the proposed device. It would make this study solid if the authors compare the software level and device level to convince the proposed devices have an advantage over software.

Response: We gratefully thanks for the precious time your spent making constructive remarks. In the second paragraph of the chapter "Spike behavior of NDR based FN neurons" of the resubmitted manuscript, we have added information about the meaning of the F-measure, explained its significance, and added relevant references to facilitate the reader's understanding. And in a new way of comparison, we compare the advantages of neuronal circuits over software operators.

Manuscript revision: "The F-Measure is a weighted summed average of accuracy and recall and is a commonly used comprehensive evaluation metric, a higher value of the F-Measure indicates a better performance in edge detection, its value ranges from 0 to 1, with 1 indicating perfect performance[33]."

Meanwhile, the FN neuron circuit performed the edge detection work using the same way as the software operator, which is the convolutional edge detection method. The edge detection was compared using two evaluation metrics, SSIM and PSNR, and the principle is demonstrated in Supplementary Information (Section 2.3). The results show that the neuron-based edge detection compared to the software operator results in SSIM of 0.949 (Roberts) and 0.933 (Sobel), shown in Fig. 5c respectively, which produces a small amount of error, but this result is acceptable. On the one hand, the software simulation is performed using a CPU for the convolution operation, which consumes about 0.0638 J of energy per convolutional computation, whereas the neuronal circuits consume 4-5 orders of magnitude less energy than the CPU for the same criteria. On the other hand, this FN neuron circuit is a basic unit circuit that can be easily embedded into other circuits to form more complex neuromorphic computing circuits to perform various real-time computational tasks, which cannot be accomplished by traditional computing chips such as CPUs.

Comment 15: Minor feedback: In Figure 5d, it would be helpful for readers to understand if the images are labeled such as original image and image from devices.

Response: We think this is a good suggestion. As recommended by reviewer 1, to better apply the high temperature resistance characteristics of the device, we replace the neuron application scenario, is a voltage temperature multimodal image recognition system, will fuse the image pixel value and temperature of the spiking signal through the spiking neural network to classify, the results show that the system produces a very good classification effect for different numbers with different temperature labels. Meanwhile, the problem described in 'Comment 15' has been solved in the new image.

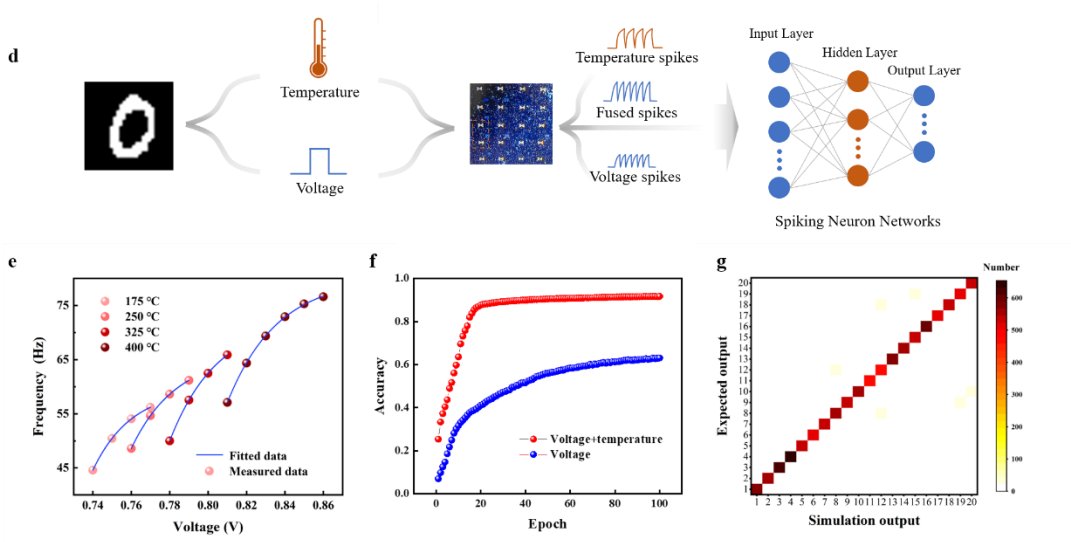

Figure R6 d, Schematic diagram of voltage-temperature multimodal image recognition system. **e**, Input voltage versus output frequency curves at four different temperatures. f, Accuracy of the network after 100 epochs using only voltage mode and voltage-temperature fusion mode. g, Confusion matrix of real and desired outputs in voltage-temperature fusion mode.

Ⅲ. Comments from Reviewer #3

The manuscript discusses the development of an ultra-robust negative differential resistance (NDR) memristor using an AlAs/In0.8Ga0.2As/AlAs quantum well structure, specifically designed for neuromorphic computing applications. This memristor is particularly noted for its high temperature resistance, high endurance, and low variation, which make it ideal for implementing hardware neuron circuits that mimic biological neuron functions. This manuscript contributes significantly to the field of neuromorphic computing, pushing the boundaries of what's possible with memristor technologies and setting a high standard for future research in this area. The integration of the NDR memristor to mimic the functionality of a neuronal membrane without the need for external capacitors is a significant advancement, potentially simplifying and reducing the cost of neuromorphic circuit design. But there are still a few issues that need to be revised and agreed to be published in Nature Communications.

Comment 1: Can the authors elaborate on the choice of the AlAs/In0.8Ga0.2As/AlAs quantum well structure over other potential materials? What specific properties of this configuration contribute to the enhanced stability and performance of the NDR memristor?

Response: The selection of AlAs/$In_{0.8}Ga_{0.2}As$/AlAs quantum well structure is based on its unique physical and chemical properties, which are crucial for the stability and performance of NDR memristors. Firstly, the lattice of AlAs matches well with InGaAs which can reduce lattice mismatch stress, thereby reducing defect density and improving device reliability[34]. Secondly, the $In_{0.8}Ga_{0.2}As$ quantum well has a narrow bandgap and can achieve electron resonance tunneling at lower voltages, thereby achieving negative differential resistance effect[35,36]. In addition, this material combination has high thermal stability, which is beneficial for maintaining device performance in high-temperature environments. Finally, by precisely controlling the ratio of In and Ga, the thickness of the quantum well and the height of the potential barrier can be adjusted, further optimizing the electron tunneling characteristics and enhancing device performance[37].

Comment 2: Given the complex fabrication process involving high-temperature epitaxial growth, how reproducible are the memristor devices across different production batches?

Response: Our manufacturing process, although involving high-temperature epitaxial

growth, has developed to a high degree of repeatability. We have adopted standardized manufacturing processes and strict quality control measures, including precise control of growth parameters and detailed performance testing after each production batch. To demonstrate the uniformity between devices from different batches, we randomly selected 10 batches of device and tested ten I-V characteristic cycle for each device as shown in Figure R9. In addition, we use in-situ monitoring technology to observe the growth process in real time, ensuring that each batch of produced memristor devices meets the design specifications.

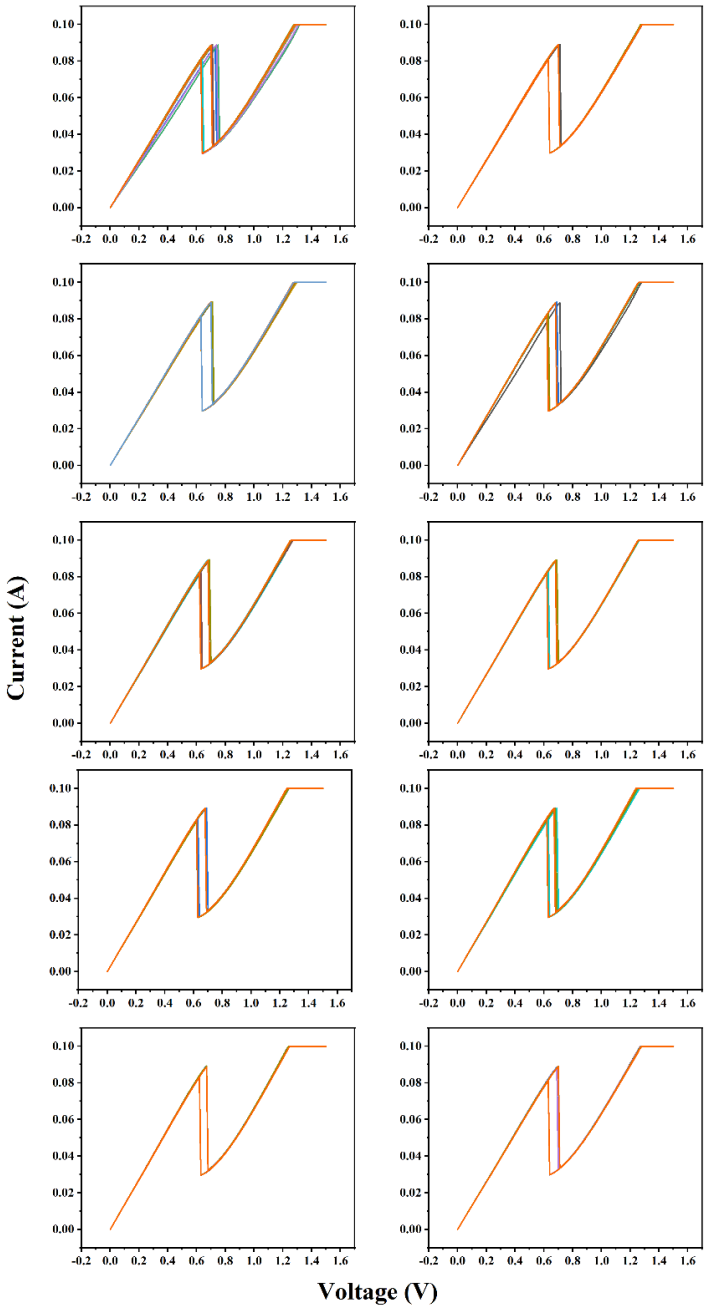

Figure R9. I-V characteristic cycle of NDR devices for different batches.

Manuscript revision:

To demonstrate the uniformity between devices from different batches, we randomly selected 10 batches of device and tested ten I-V characteristic cycle for each device. Fig. S8 showed that the devices from different batches had good uniformity.

Comment 3: How does the device maintain its integrity and performance over prolonged exposure to harsh environmental conditions?

Response: For the NDR devices in this work, ultra robust performance was achieved through optimized growth, indicating that high yield devices can be achieved in large-scale production. The high-quality AlAs/$In_{0.8}Ga_{0.2}As$/AlAs quantum well structure grown by MOVPE technology ensures the high quality and crystal integrity of materials. The accurate composition of $In_{0.8}Ga_{0.2}As$ alloy is achieved by precisely controlling the flow rate of III-V precursors, reducing lattice mismatch. In situ monitoring techniques such as RHEED were used to observe the growth process in real time and adjust the parameters in time to optimize the film quality. In the future large-scale production, protective packaging technology may be used to prevent physical damage and environmental factors such as humidity, chemical corrosion, etc. from affecting device performance. The test results show that the NDR device has indeed achieved good stability at high temperatures, and can maintain stable I-V characteristics even at high temperatures up to 400 °C. After more than 10^9 cycle tests at high temperature, it shows excellent durability and stability.

Comment 4: How does the simplification of the FN neuron circuit, achieved by using only two NDR memristors and an inductor, affect the circuit's ability to replicate more complex neuron behaviors? The author can provide a more detailed description in this section.

Response: This simplified circuit design benefits from the N-type negative differential resistance characteristics of NDR devices, which are very suitable for FN neuron circuits. The collaborative process of two NDR devices in neuromorphic circuits is significantly like the generation and propagation of action potentials in real neurons. In real neurons, the generation of action potentials is caused by the dynamic opening and closing of voltage-gated sodium and potassium ion channels, while the depolarization and hyperpolarization stages are controlled by the flow of sodium and potassium ions, respectively. Similarly, in our circuit, two NDR devices simulate the behavior of these ion channels: 1. In the resting state, both devices are in

a LRS state, which corresponds to the resting state of neuronal membrane potential. 2. The depolarization, when the input voltage exceeds the oscillation voltage of D1, which will be triggered to the oscillation state. Due to the voltage division principle between the device and the inductor, the node voltage will increase, and D2 will be triggered to the oscillation state, causing the node voltage to rise again. 3. Afterwards, due to the presence of inductance, the node voltage will gradually decrease until D2 can be converted back to LRS. This will lead to a decrease in the partial voltage of the device, and the node voltage will also decrease, causing the state of D1 to return to LRS. At this point, the node voltage will become negative, corresponding to the processes of repolarization and hyperpolarization. 4. Because of inductance, the node voltage will slowly return to the resting potential. This corresponds to the refractory period. By precisely adjusting the characteristics of NDR devices, multiple discharge behaviors and the integration and synchronous oscillation behavior of complex neural networks can be achieved as shown in Figure R10 (Figure 4 in manuscript).

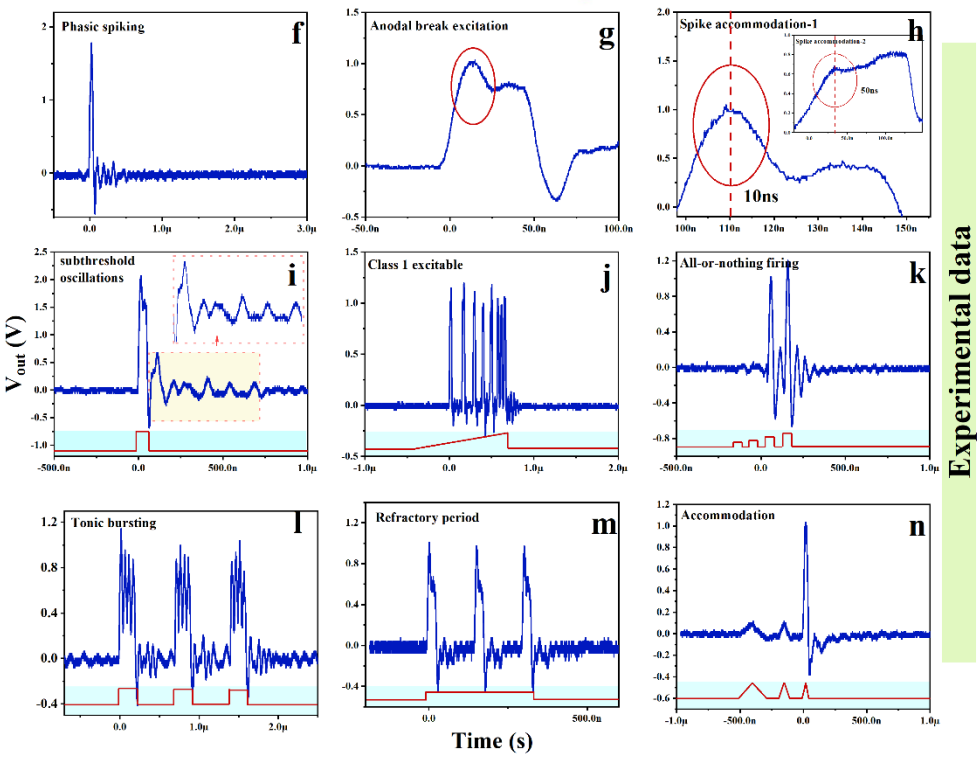

Figure R10. Biological neuron behavior modeling and experimental measurement.

Comment 5: There is a duplicate image between Fig S14 and Fig 5, and one of them needs to be deleted.

Response: Thank you for your reminder. Based on the suggestion of Reviewer 1, we have

revised Fig 5. To better apply the high temperature resistance characteristics of the device, we replace the neuron application scenario, is a voltage temperature multimodal image recognition system, will fuse the image pixel value and temperature of the spiking signal through the spiking neural network to classify, the results show that the system produces a very good classification effect for different numbers with different temperature labels. Meanwhile, the problem described in 'Comment 5' has been solved in the new image.

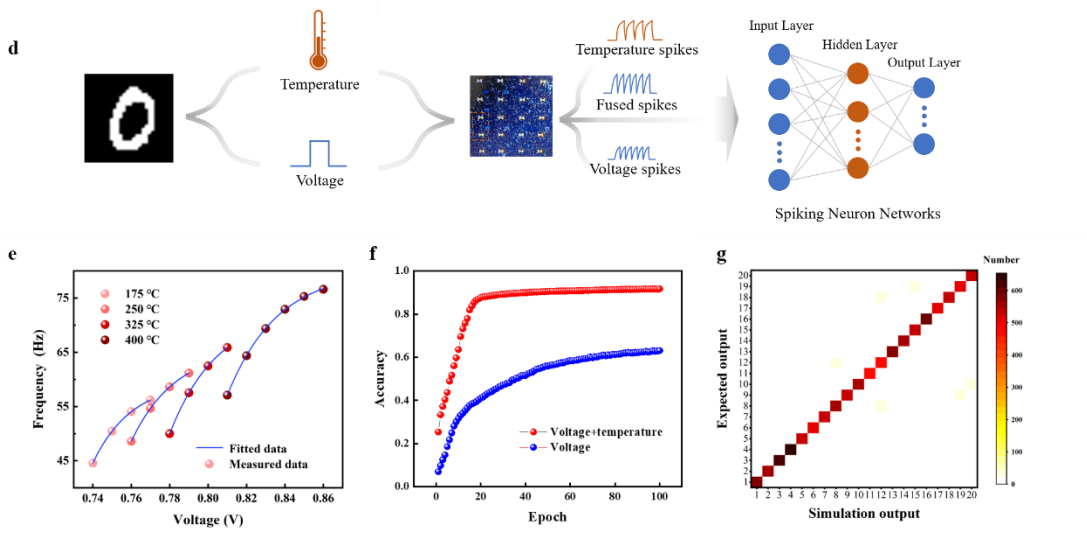

Figure R6 d, Schematic diagram of voltage-temperature multimodal image recognition system. **e**, Input voltage versus output frequency curves at four different temperatures. f, Accuracy of the network after 100 epochs using only voltage mode and voltage-temperature fusion mode. g, Confusion matrix of real and desired outputs in voltage-temperature fusion mode.

References

1 Wang, Z. *et al.* Fully memristive neural networks for pattern classification with unsupervised learning. *Nature Electronics* **1**, 137-145 (2018).

2 Tuma, T., Pantazi, A., Le Gallo, M., Sebastian, A. & Eleftheriou, E. Stochastic phase-change neurons. *Nature nanotechnology* **11**, 693-699 (2016).

3 Pickett, M. D., Medeiros-Ribeiro, G. & Williams, R. S. A scalable neuristor built with Mott memristors. *Nature materials* **12**, 114-117 (2013).

4 Yan, X. *et al.* Self-assembled networked PbS distribution quantum dots for resistive switching and artificial synapse performance boost of memristors. *Advanced materials* **31**, 1805284 (2019).

5 Pei, Y. *et al.* Artificial visual perception nervous system based on low-dimensional material photoelectric memristors. *ACS nano* **15**, 17319-17326 (2021).

6 Zhao, J. *et al.* Realization of long retention properties of quantum conductance through confining the oxygen vacancy diffusion. *Applied Physics Reviews* **9** (2022).

7 Ortega-Piwonka, I., Piro, O., Figueiredo, J., Romeira, B. & Javaloyes, J. Bursting and excitability in neuromorphic resonant tunneling diodes. *Physical Review Applied* **15**, 034017

(2021).

8 Hasan, R. M. M. & Luo, X. Promising lithography techniques for next-generation logic devices. *Nanomanufacturing and Metrology* **1**, 67-81 (2018).

9 Jensen, K. F., Fotiadis, D. I. & Mountziaris, T. J. Detailed models of the MOVPE process. *Journal of crystal growth* **107**, 1-11 (1991).

10 Bean, B. P. The action potential in mammalian central neurons. *Nature Reviews Neuroscience* **8**, 451-465 (2007).

11 Tu, X., Mikaelian, G. & Ho, W. Controlling Single-Molecule Negative Differential Resistance in a Double-Barrier Tunnel Junction. *Physical review letters* **100**, 126807 (2008).

12 Wang, H., Wu, Y., Cong, C., Shang, J. & Yu, T. Hysteresis of electronic transport in graphene transistors. *ACS nano* **4**, 7221-7228 (2010).

13 Burstein, L., Bregman, J. & Shapira, Y. Surface photovoltage spectroscopy of gap states at GaAs and InP metal interfaces. *Applied physics letters* **57**, 2466-2468 (1990).

14 Ganose, A. M. *et al.* Efficient calculation of carrier scattering rates from first principles. *Nature communications* **12**, 2222 (2021).

15 Luckyanova, M. N. *et al.* Anisotropy of the thermal conductivity in GaAs/AlAs superlattices. *Nano letters* **13**, 3973-3977 (2013).

16 Zhang, Y. *et al.* Evolution of the conductive filament system in HfO2-based memristors observed by direct atomic-scale imaging. *Nature communications* **12**, 7232 (2021).

17 Cassinerio, M., Ciocchini, N. & Ielmini, D. Logic computation in phase change materials by threshold and memory switching. *Advanced Materials* **25**, 5975-5980 (2013).

18 Hou, W. *et al.* Strain engineering of vertical molybdenum ditelluride phase-change memristors. *Nature Electronics* **7**, 8-16 (2024).

19 Boucart, K. & Ionescu, A. M. Double-gate tunnel FET with high-kappa gate dielectric. *IEEE transactions on electron devices* **54**, 1725-1733 (2007).

20 Balestra, F., Cristoloveanu, S., Benachir, M., Brini, J. & Elewa, T. Double-gate silicon-on-insulator transistor with volume inversion: A new device with greatly enhanced performance. *IEEE Electron Device Letters* **8**, 410-412 (1987).

21 Park, S.-O., Jeong, H., Park, J., Bae, J. & Choi, S. Experimental demonstration of highly reliable dynamic memristor for artificial neuron and neuromorphic computing. *Nature Communications* **13**, 1-13 (2022).

22 Lee, J. H., Chiang, J.-C., Li, S. S. & Kannam, P. An AlAs/InGaAs/AlAs/InAlAs double-barrier quantum well infrared photodetector operating at 3.4 μm and 205 K. *Applied physics letters* **74**, 765-767 (1999).

23 Ohya, S., Hai, P. N. & Tanaka, M. Tunneling magnetoresistance in GaMnAs⁄ AlAs⁄ InGaAs⁄ AlAs⁄ GaMnAs double-barrier magnetic tunnel junctions. *Applied Physics Letters* **87** (2005).

24 Grabert, H., Weiss, U. & Hanggi, P. Quantum tunneling in dissipative systems at finite temperatures. *Physical review letters* **52**, 2193 (1984).

25 Kluksdahl, N., Kriman, A., Ferry, D. & Ringhofer, C. Self-consistent study of the resonant-tunneling diode. *Physical Review B* **39**, 7720 (1989).

26 Fu, T. *et al.* Bioinspired bio-voltage memristors. *Nature communications* **11**, 1861 (2020).

27 Gorbachev, R. V., Mayorov, A. S., Savchenko, A. K., Horsell, D. W. & Guinea, F. Conductance of pnp graphene structures with “air-bridge” top gates. *Nano letters* **8**, 1995-1999 (2008).

28 Kawai, N. *et al.* Confined band gap in an air-bridge type of two-dimensional AlGaAs photonic

crystal. *Physical review letters* **86**, 2289 (2001).

29 Kumar, S., Strachan, J. P. & Williams, R. S. Chaotic dynamics in nanoscale NbO_2 Mott memristors for analogue computing. *Nature* **548**, 318-321 (2017).

30 Baek, Y.-H. *et al.* 94-GHz log-periodic antenna on GaAs substrate using air-bridge structure. *IEEE Antennas and Wireless Propagation Letters* **8**, 909-911 (2009).

31 Lu, Y. *et al.* An electronic silicon-based memristor with a high switching uniformity. *Nature Electronics* **2**, 66-74 (2019).

32 Petrovas, A., Lisauskas, S. & Slepikas, A. Electronic model of fitzhugh-nagumo neuron. *Elektronika ir elektrotechnika* **122**, 117-120 (2012).

33 Liu, Y., Cheng, M.-M., Hu, X., Wang, K. & Bai, X. in *Proceedings of the IEEE conference on computer vision and pattern recognition.* 3000-3009.

34 Muttlak, S. G., Abdulwahid, O. S., Sexton, J., Kelly, M. J. & Missous, M. InGaAs/AlAs resonant tunneling diodes for THz applications: an experimental investigation. *IEEE Journal of the Electron Devices Society* **6**, 254-262 (2018).

35 Hausser, S., Fuchs, G., Hangleiter, A., Streubel, K. & Tsang, W. Auger recombination in bulk and quantum well InGaAs. *Applied physics letters* **56**, 913-915 (1990).

36 Van Eck, T., Chu, P., Chang, W. & Wieder, H. Electroabsorption in an InGaAs/GaAs strained-layer multiple quantum well structure. *Applied physics letters* **49**, 135-136 (1986).

37 Karunasiri, G. Thermionic emission and tunneling in InGaAs/GaAs quantum well infrared detectors. *Journal of applied physics* **79**, 8121-8123 (1996).

Thank you for the detailed response to the comments. Authors had addressed most of the questions from this reviewer but there are still few questions remaining. The following questions and suggestions should be addressed before publication.

1. Authors have updated abstract and Figure R1 which are related to the durability of proposed NDR device. However, this reviewer wonders why authors only test 10^9 cycles at 400 ℃ while 10^11 cycles at room temperature. Is there any unexpected result observed after 10^9 cycles at 400 ℃? In the cyclic test at 400 ℃ graph, there is fluctuation of peak current as the cycles repeated while there is no fluctuation in peak current at room temperature. Authors should discuss about this phenomenon in the manuscript. In addition, this reviewer recommends to mention about the expected lifetime (310 years) in the abstract which could appeal the strength of proposed NDR device more effectively.
2. Since the longer lifetime of the proposed NDR device is the key strength, this reviewer suggests to add the lifetime comparison with other preliminary studies in the revised table R1.

REVIEWER COMMENTS

Reviewer #2 (Remarks to the Author):

I appreciate the authors for giving thorough replies and revisions to my comments. However, there are still a few things to be clarified and need more details. Below are the follow-up comments from my original comment and additional comments from revisions the authors provided.

1. From the original comment 1 and the manuscript revision, when it comes to resonant tunneling diode (RTD), the sentence " preparation process is relatively mature ~" still gives ambiguous expression. The authors are recommended to compare how they are considered the other conventional NDR devices.

2. From the original comment 6, could you provide an example of NDR devices having different characteristics by controlling the growth conditions or process steps?

3. From the original comment 11, the authors provides the Figure R5 to provide the details on hysteresis range of NDR devices (unstable state), however, Figure R5 shows the illustration of proposed devices and SEM image of air bridge. It would be great if the authors can provide appropriate figure to give details on that.

4. From the original comment 13 and manuscript revision, the authors provided the computation energy of convolution operation with CPU and neuronal circuits. It would be more convincing if the authors can provide how they calculate the computation energy consumed by two different operations. The "same criteria" the authors mentioned are insufficient to compare the two operations.

5. In figure 4 i-k, please provide what the plotting in red presents and clarify their voltage amplitude and sign. In supplementary figure S14, which presents the simulation results to verify, the input is positive voltage, however, the experimental results look like the red plot is minus (assumed red plot is input as well).

6. "In Figures 5d-g, additional background is required to demonstrate the voltage-temperature fused multimodal spiking neural network system. For example, it would be helpful to explain why this system has been demonstrated (introduction of temperature wise) and how the proposed NDR contributes to reliable neuromorphic computing, especially considering that numerous studies regarding memristors have already classified the MNIST dataset.

Reviewer #3 (Remarks to the Author):

I co-reviewed this manuscript with one of the reviewers who provided the listed reports. This is part of the Nature Communications initiative to facilitate training in peer review and to provide appropriate recognition for Early Career Researchers who co-review manuscripts.

Reviewer #4 (Remarks to the Author):

I have checked the revised version of the paper by Yan et al. The authors have carefully answered the questions raised by the reviewers and revised the manuscript with much necessary data and comments included. The rewritten contents and discussion of the revised manuscript look much better. Therefore, I think this revised manuscript adequately addressed the reviewers' request. It meets the high standards of NC and is suitable for publication now.

Dear Reviewers and Editor:

Thank you for the reviewers' comments concerning our manuscript entitled "**Ultra robust negative differential resistance memristor for hardware neuron circuit implementation**" **(NCOMMS-24-25158-A)**. Those comments are all valuable and very helpful for revising and improving our paper, as well as the important guiding significance to our research. We have studied comments carefully and have made correction which we hope meet with approval. Revised portions are marked in red in the paper. The main corrections in the manuscript and the responds to the reviewer's comments are as following:

l. Reviewer #1 (Remarks to the Author):

Thank you for the detailed response to the comments. Authors had addressed most of the questions from this reviewer but there are still few questions remaining. The following questions and suggestions should be addressed before publication.

Response: Thank you very much for commenting the significance of our work and giving us insightful suggestions to further improve the quality of this work. Our responses to your specific comments one by one are shown as follows.

Comment 1: Authors have updated abstract and Figure R1 which are related to the durability of proposed NDR device. However, this reviewer wonders why authors only test 10^9 cycles at 400 ℃ while 10^11 cycles at room temperature. Is there any unexpected result observed after 10^9 cycles at 400 ℃? In the cyclic test at 400 ℃ graph, there is fluctuation of peak current as the cycles repeated while there is no fluctuation in peak current at room temperature. Authors should discuss about this phenomenon in the manuscript. In addition, this reviewer recommends to mention about the expected lifetime (310 years) in the abstract which could appeal the strength of proposed NDR device more effectively.

Response: The current fluctuation range of the device after 10^9 cycles of testing at 400 ℃ was 5.04% ($\triangle I/I_{mean}$), exceeding our expected 5%[1]. Continuing the testing may result in a wider range of current fluctuations. In addition, prolonged exposure to high temperatures on the probe station may affect its lifespan and testing safety, so we manually stopped the testing, after 10^9 cycles.

Under normal circumstances, maintaining stability in a high-temperature testing

environment may be more difficult than in a room temperature environment. On the one hand, NDR memristor is based on the AlAs/$In_{0.8}Ga_{0.2}As$/AlAs quantum well (QW) structure, which may exhibit better electron tunneling properties at high temperatures because thermal energy increases the probability of electrons crossing the potential barrier. This effect may be more significant at high temperatures, leading to fluctuations in peak current. On the other hand, high temperatures may alter the number and energy distribution of interface and defect states, which can capture or release charge carriers and affect the current of the device. Although this work uses control device technology to minimize the formation of interface states as much as possible. However, in high-temperature cycling tests, even small interface state changes may be amplified, leading to fluctuations in peak current.

Finally, thank you for your professional advice. We have added a description in the abstract that the device is expected to work for 310 years and have marked the changes in the manuscript.

Manuscript revision:

The NDR devices can cycle more than 10^{11} switching cycles at room temperature and more than 10^{9} switching cycles even at a high temperature of 400°C, which means that the device can operate for more than 310 years at 10 Hz update frequency.

Comment 2: Since the longer lifetime of the proposed NDR device is the key strength, this reviewer suggests to add the lifetime comparison with other preliminary studies in the revised table R1.

Response: Thank you for your valuable suggestion. We understand your interest in having a lifetime comparison with other preliminary studies in the revised Table R1 to highlight the longevity advantage of our proposed NDR device. However, Lifetime is related to endurance, so we explain lifetime by comparing endurance. Therefore, to ensure the accuracy and consistency of the comparison, we have chosen to compare the explicitly reported "endurance" data from various studies. As shown in the Table R1, our device features highest endurance, indicating the highest lifetime.

Table S1. Comparison of performance with threshold switching devices used in neural circuits in recent years.

Material system	Endurance	Variation	Neuronal complexity	Turn-on time	Turn-off time	Ref
Ag/SiO_2/Au	-		3	-	-	2
Au/VO_2/Au	6.5×10^6	0.73%	3	<70ns	<60ns	3
Pt/Ti/NbO_x/Pt/Ti	50		2	<50ns	<25ns	4
Pt/CuS/GeSe/Pt	1.8×10^6		3	200ns	~3μs	5
Pd/Ag/HfO_x/Ag/Pd	1×10^8			75ns	250ns	6
Ag/ZrO_x/Pt	200	5.56%	-	-	-	7
Au/Ag/hBN/Au/Ti	500	37.5%	3	-	-	8
Ag/WSe_2/Ag	1×10^4		-	700ns	-	9
Au/$CH_3NH_3PbI_3$/ITO	-		8	-	-	10
Pt/VO_2/Pt	2.66×10^7		4	-	-	11
Pt/PEDOT:PSS/WO_3/W	-		4	-	-	12
Pt/SiO_2(Ag)/SiO_2/Pt	-		3		<1ms	13
Pt/Ti/NbO_x/Pt	-		2	-	-	14
Pt/AgGeSe/Al_2O_3/Pt	-	2.18%	-	<300ns	<30μs	15
Ag/TiN/HfO_x/HfO_y/HfO_z/Pt	1×10^6	5.4%	-	60ns	500ns	16
Ag/Si/Pt	-		3	20ns	16ns	17
This work	1×10^{11}	0.295%	1	10ns	50ns	

Ⅱ. Reviewer #2 (Remarks to the Author):

I appreciate the authors for giving thorough replies and revisions to my comments. However, there are still a few things to be clarified and need more details. Below are the follow-up comments from my original comment and additional comments from revisions the authors provided.

Comment 1: From the original comment 1 and the manuscript revision, when it comes to resonant tunneling diode (RTD), the sentence " preparation process is relatively mature ~" still gives ambiguous expression. The authors are recommended to compare how they are considered the other conventional NDR devices.

Response: Thanks for your suggestion. Usually, FN neural circuits require N-type negative differential resistance (NDR) memristors to be implemented[18], while traditional S-type NDR memristors including threshold switch memristors[19], phase change memristors (PCM)[20], and Mott memristors[21] are difficult to support the implementation of FN neural circuits. On the other hand, PCM and Mott memristors will undergo volume changes during the resistance change process, and the nucleation sites of conductive filament type memristors have random paths, making it difficult for the devices to have good uniformity and repeatability[22-24]. Therefore, finding more stable N-type NDR devices to construct neural circuits is a very necessary task. Fortunately, the resonant tunneling diode (RTD) is a typical N-type NDR device that adopts band controlled tunneling mechanism and is less affected by temperature, which makes it have better device stability[25].

Comment 2: From the original comment 6, could you provide an example of NDR devices having different characteristics by controlling the growth conditions or process steps?

Response: Thank you for your professional question. In this experiment, when growing $In_{0.8}Ga_{0.2}As$ quantum wells at a growth rate of 4 nm/min, the atoms have enough time to align in the lattice to grow thin films with fewer defects. At the same time, the NDR device does not exhibit significant box hysteresis characteristics as shown in Fig R1. We would consider increasing the growth rate to 6 nm/min and artificially introducing defects to produce box type hysteresis characteristics to meet the requirements of neuronal circuits.

In addition, device size and tunnel layer thickness also have an impact on device voltage

parameters. For example, the smaller the device size, the higher the switching voltage, and the thicker the tunneling layer, the higher the switching voltage.

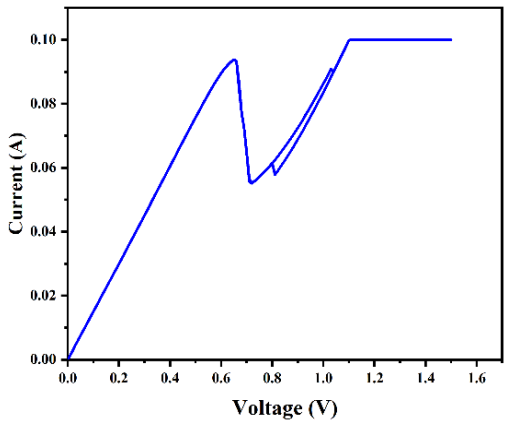

Figure R1. I-V curves of NDR devices with reduced lattice defects.

Comment 3: From the original comment 11, the authors provides the Figure R5 to provide the details on hysteresis range of NDR devices (unstable state), however, Figure R5 shows the illustration of proposed devices and SEM image of air bridge. It would be great if the authors can provide appropriate figure to give details on that.

Response: We apologize for our mistake on labeling the image number. The correct Figure R5, as shown in Figure R2, represents an "unstable state" indicating that the working state of the NDR device is within the hysteresis range. Thank you for your careful review.

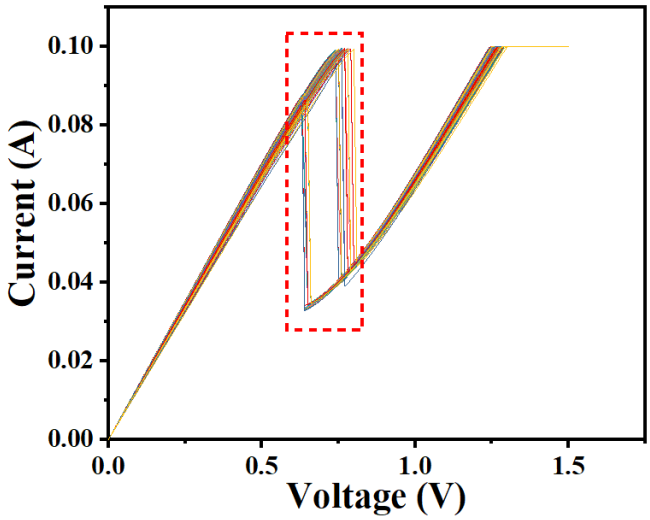

Figure R2. The red circle indicates that the working status of the NDR device is within the hysteresis range.

Comment 4: From the original comment 13 and manuscript revision, the authors provided the computation energy of convolution operation with CPU and neuronal circuits. It would be

more convincing if the authors can provide how they calculate the computation energy consumed by two different operations. The "same criteria" the authors mentioned are insufficient to compare the two operations.

Response: We apologize for causing you with confusion. We mentioned the "same criterion" to mean that when calculating the power consumption, the power consumption of the two different approaches (software operators and neuron circuits) is the amount of energy consumed by a single convolutional operation using 3*3 convolutional kernels. According to your suggestion, we revised the description of the relevant parts of the manuscript to explain in detail how the power consumption of the CPU and neuronal circuits is calculated.

For edge detection of an image using software operators, we used MATLAB for the estimation, and part of the code and running results are shown in Fig. R3. We use the Sobel operator to perform edge detection on an image, record the CPU occupancy and execution time during the execution of edge detection, and also calculate the number of times the convolution operation is performed, which results in an average power of 8.7583W to perform the entire convolution operation, an execution time of 1.0167s, and a total number of convolutions performed of 64,516, which ultimately estimates the power consumption of performing a

convolution operation is about 138.02uJ.

```
img = imread('image.png');
grayImg = img;
monitorInterval = 0.01;
monitorCount = 10;
initialCpuUsage = zeros(monitorCount, 1);
finalCpuUsage = zeros(monitorCount, 1);
maxPower = 115;
for i = 1:monitorCount
    [status, result] = system('powershell -command "Get-WmiObject -Class Win32_PerfFormattedData_
    if status == 0
        data = str2double(regexp(result, '\d+', 'match'));
        initialCpuUsage(i) = mean(data);
    else
        disp('Error in fetching power consumption');
    end
    pause(monitorInterval);
end

avgInitialCpuUsage = mean(initialCpuUsage);
tic;
edgesSobel = edge(grayImg, 'Sobel');
figure;
subplot(2, 3, 1);
imshow(img);
title('original image');

subplot(2, 3, 2);
imshow(edgesSobel);
title('Sobel image');

elapsedTime = toc;
```

```
Total Convolution Operations: 64516
Initial Power Consumption: 7.3364 %
Final Power Consumption: 7.8955 %
Elapsed Time: 1.0167 seconds
Average Power Consumption During Process: 8.7583 W
>>
```

Figure R3. Part of the code for estimating the energy consumption for performing convolution operations using MATLAB

For edge detection operation using neuronal circuitry, the power consumption is obtained from the following equation

$$\boldsymbol{P = V * I \int_{t_0}^{t_1} t}$$

Where t_0 and t_1 are the time of the start and end of one oscillation of the neuron circuit, respectively, P in the above equation is the power consumption of the neuron to perform one operation, and one convolution operation performs 9 operations, which ultimately yields the energy consumption of the neuron circuit for one convolution operation to be 4.11nJ.

Manuscript revision:

On one hand, the convolution operation performed by software is executed on the CPU. The energy consumption of the CPU and neuron circuits during the edge detection process was assessed (Both calculate the energy consumed to complete a convolution operation using a 3*3 convolution kernel), the MATLAB-based estimation determined that the energy consumption for the CPU to perform a single convolution operation is approximately 138.02 μJ, whereas the neuron circuits consume about 4.11 nJ for the same task. This represents an energy reduction of 5 to 6 orders of magnitude when using neuron circuits compared to the CPU

Comment 5: In figure 4 i-k, please provide what the plotting in red presents and clarify their voltage amplitude and sign. In supplementary figure S14, which presents the simulation results to verify, the input is positive voltage, however, the experimental results look like the red plot is minus (assumed red plot is input as well).

Response: We apologize for any misunderstanding caused by our graphic representation. The red lines in Figure 4 i-k represent the schematic diagram of the input waveform and do not correspond to the coordinate axis voltage values. In order to express it more clearly, we have revised Figure 4.

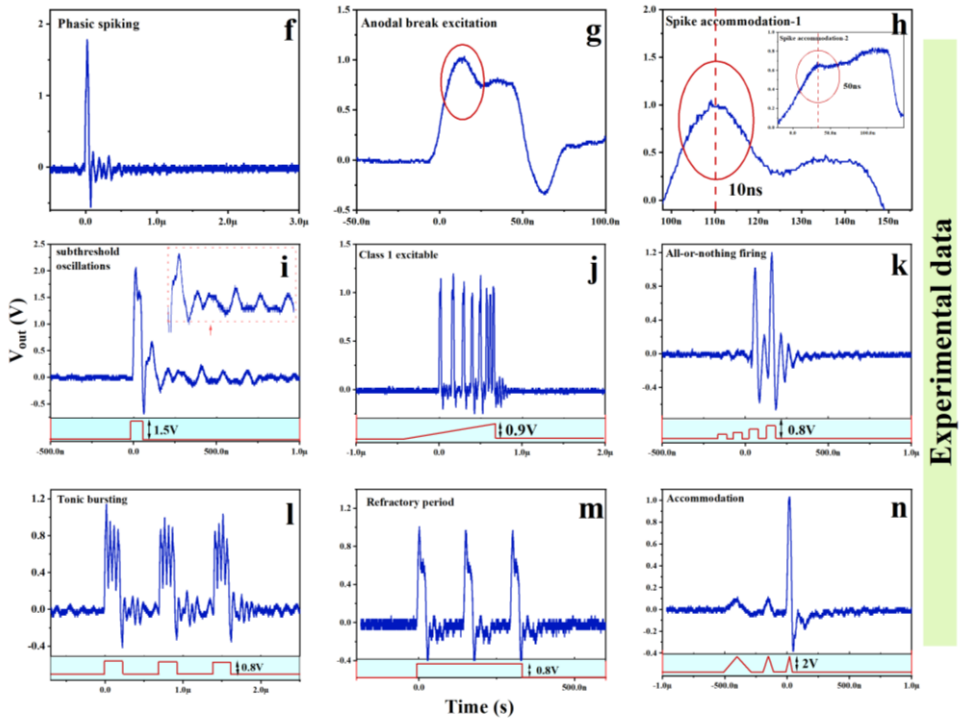

Fig. 4 f-n, The experiment demonstrated 9 biological neuron spike behaviors in FN neuron circuits based on NDR memristors. **f**, phasic spiking, **g**, anodal break excitation, **h**, spike accommodation, **i**, subthreshold oscillations, **j**,

class 1 excitable, **k**, all or nothing firing, **l**, tonic bursting, **m**, refractory period, **n**, accommodation.

Comment 6: "In Figures 5d-g, additional background is required to demonstrate the voltage-temperature fused multimodal spiking neural network system. For example, it would be helpful to explain why this system has been demonstrated (introduction of temperature wise) and how the proposed NDR contributes to reliable neuromorphic computing, especially considering that numerous studies regarding memristors have already classified the MNIST dataset.

Response: Thanks for your professional question. As you are concerned, many studies on memristors have classified the MNIST dataset, however, our work is more of a demonstration of the stability properties of the proposed NDR device at high temperatures. We processed the MNIST dataset by artificially introducing the information of temperature dimension and compared the accuracy of the classification of the spiking neural network based on the proposed NDR device under two different datasets (the original MNIST and the MNIST with the introduction of the temperature information), which is something that is not available in other studies involving memristors on the MNIST dataset.

Our results show that, due to the high-temperature stability of NDR devices, our proposed voltage-temperature fusion multimodal spiking neural network system can achieve robust classification results for handwritten digit images with varying temperature labels. This demonstrates the potential of our NDR devices for reliable neuromorphic computation in high-temperature environments.

Ⅲ. Reviewer #3 (Remarks to the Author):

I co-reviewed this manuscript with one of the reviewers who provided the listed reports. This is part of the Nature Communications initiative to facilitate training in peer review and to provide appropriate recognition for Early Career Researchers who co-review manuscripts.

Response: Thank you very much for your participation in the peer review process. We appreciate the collaborative effort in reviewing our manuscript.

Ⅳ. Reviewer #4 (Remarks to the Author):

I have checked the revised version of the paper by Yan et al. The authors have carefully answered the questions raised by the reviewers and revised the manuscript with much necessary data and comments included. The rewritten contents and discussion of the revised manuscript look much better. Therefore, I think this revised manuscript adequately addressed the reviewers' request. It meets the high standards of NC and is suitable for publication now.

Response: Thank you very much for recommending the publication of our manuscript. We sincerely appreciate your valuable time and effort in reviewing our work.

References

1 Goswami, S. *et al.* Robust resistive memory devices using solution-processable metal-coordinated azo aromatics. *Nature materials* **16**, 1216-1224 (2017).

2 Zhang, X. *et al.* An artificial neuron based on a threshold switching memristor. *IEEE Electron Device Letters* **39**, 308-311 (2017).

3 Yuan, R. *et al.* A neuromorphic physiological signal processing system based on VO2 memristor for next-generation human-machine interface. *Nature Communications* **14**, 3695 (2023).

4 Duan, Q. *et al.* Spiking neurons with spatiotemporal dynamics and gain modulation for monolithically integrated memristive neural networks. *Nature communications* **11**, 3399 (2020).

5 Wang, K. *et al.* Threshold switching memristor-based stochastic neurons for probabilistic computing. *Materials Horizons* **8**, 619-629 (2021).

6 Midya, R. *et al.* Anatomy of Ag/Hafnia-based selectors with 10 10 nonlinearity. *Advanced Materials* **29** (2017).

7 Yang, J. H., Mao, S. C., Chen, K. T. & Chen, J. S. Emulating Nociceptive Receptor and LIF Neuron Behavior via ZrOx-based Threshold Switching Memristor. *Advanced Electronic Materials* **9**, 2201006 (2023).

8 Jo, Y. *et al.* Hardware Implementation of Network Connectivity Relationships Using 2D hBN-Based Artificial Neuron and Synaptic Devices. *Advanced Functional Materials* **34**, 2309058 (2024).

9 Sivan, M. *et al.* All WSe2 1T1R resistive RAM cell for future monolithic 3D embedded memory integration. *Nature communications* **10**, 5201 (2019).

10 Yang, J.-Q. *et al.* Leaky integrate-and-fire neurons based on perovskite memristor for spiking

neural networks. *Nano Energy* **74**, 104828 (2020).

11 Yi, W. *et al.* Biological plausibility and stochasticity in scalable VO2 active memristor neurons. *Nature communications* **9**, 4661 (2018).

12 Huang, H. M. *et al.* Quasi-Hodgkin–Huxley Neurons with Leaky Integrate-and-Fire Functions Physically Realized with Memristive Devices. *Advanced Materials* **31**, 1803849 (2019).

13 Ye, F., Kiani, F., Huang, Y. & Xia, Q. Diffusive Memristors with Uniform and Tunable Relaxation Time for Spike Generation in Event-Based Pattern Recognition. *Advanced Materials* **35**, 2204778 (2023).

14 Kim, G. *et al.* Self-clocking fast and variation tolerant true random number generator based on a stochastic mott memristor. *Nature communications* **12**, 2906 (2021).

15 Wan, T.-Q. *et al.* 12.7 MA/cm 2 on-current density and high uniformity realized in AgGeSe/Al 2 O 3 selectors. *IEEE Electron Device Letters* **42**, 613-616 (2021).

16 Lu, Y. F. *et al.* A high-performance Ag/TiN/HfOx/HfOy/HfOx/Pt diffusive memristor for calibration-free true random number generator. *Advanced Electronic Materials* **8**, 2200202 (2022).

17 Yan, L. *et al.* High-speed Si films based threshold switching device and its artificial neuron application. *Applied Physics Letters* **119** (2021).

18 Ahsan, R., Wu, Z., Jalal, S. A. A. & Kapadia, R. Ultralow Power Electronic Analog of a Biological Fitzhugh–Nagumo Neuron. *ACS omega* **9**, 18062-18071 (2024).

19 Wang, Z. *et al.* Fully memristive neural networks for pattern classification with unsupervised learning. *Nature Electronics* **1**, 137-145 (2018).

20 Tuma, T., Pantazi, A., Le Gallo, M., Sebastian, A. & Eleftheriou, E. Stochastic phase-change neurons. *Nature nanotechnology* **11**, 693-699 (2016).

21 Pickett, M. D., Medeiros-Ribeiro, G. & Williams, R. S. A scalable neuristor built with Mott memristors. *Nature materials* **12**, 114-117 (2013).

22 Yan, X. *et al.* Self-assembled networked PbS distribution quantum dots for resistive switching and artificial synapse performance boost of memristors. *Advanced materials* **31**, 1805284 (2019).

23 Pei, Y. *et al.* Artificial visual perception nervous system based on low-dimensional material photoelectric memristors. *ACS nano* **15**, 17319-17326 (2021).

24 Zhao, J. *et al.* Realization of long retention properties of quantum conductance through confining the oxygen vacancy diffusion. *Applied Physics Reviews* **9** (2022).

25 Ortega-Piwonka, I., Piro, O., Figueiredo, J., Romeira, B. & Javaloyes, J. Bursting and excitability in neuromorphic resonant tunneling diodes. *Physical Review Applied* **15**, 034017 (2021).

REVIEWERS' COMMENTS

Reviewer #1 (Remarks to the Author):

The authors have answered all the questions raised by this reviewer and revised the manuscript. Therefore, this reviewer recommend this revised manuscript to be published in Nature Communications.

Reviewer #2 (Remarks to the Author):

Authors address all the raised comments, so I would recommend the manuscript published in Nature communications.

Reviewer #3 (Remarks to the Author):

I co-reviewed this manuscript with one of the reviewers who provided the listed reports. This is part of the Nature Communications initiative to facilitate training in peer review and to provide appropriate recognition for Early Career Researchers who co-review manuscripts.

The authors have answered all the questions raised by this reviewer and revised the manuscript. Therefore, this reviewer recommend this revised manuscript to be published in *Nature Communications*.